Spatial non-uniformity of stress in the forearc region: an example of the middle Miocene southwest Japan arc

Noriaki Abe

Doctoral Dissertation

Department of Geology and Mineralogy
Division of Earth and Planetary Sciences
Graduate School of Science
Kyoto University

December, 2022

前弧域の応力の空間的非一様性：中期中新世西南日本弧の例

安邊　啓明

博士論文

京都大学大学院理学研究科
地球惑星科学専攻
地質学鉱物学分野

令和4年(2022年)12月

Abstract

In the present forearc regions, stress varies spatially by subduction-related deformations and spatial variation of physical properties. However, it has yet been doubtful whether such stress variation could be recorded as deformation structures and whether we could detect such a stress variation in the paleo-forearc region. Plural Miocene forearc basin deposits exist in southwest Japan, and they are suitable for verifying spatial non-uniformity of stress in the forearc region with a geologic time scale. Additionally, recent studies reported the data against the conventional description that southwest Japan had changed from extension to N–S shortening at approximately 15 Ma. Although the data suggested spatial variation of stresses, those in the forearc region are limited. Thus, it is expected to reveal detailed stress in the period. Therefore, this study aims to elucidate the spatiotemporal stress variation in the forearc region in the middle Miocene southwest Japan.

In the lower-middle Miocene Tanabe Group in the southwest Kii Peninsula, this study measured the attitudes of 1124 clastic dikes, 402 calcite veins, and 426 outcrop-scale faults and then applied paleo-stress analyses. After the analyses, hierarchical clustering is applied to the detected stresses. As a result, this study estimated the following three stresses: (i) stresses with E–W trending minimum principal stress axis exerted between 16–15 Ma, (ii) stresses with NW–SE trending maximum horizontal compression axis exerted after 15 Ma, and NW–SE tension stresses only acting in the southern Tanabe Group after 15 Ma. In the lower Miocene Kurami Group in central Shizuoka Prefecture, 229 outcrop-scale faults were measured and analyzed. Additionally, based on the tilt correcting test, this study examined the timing of stresses with reference to 16 Ma fold formation. It was concluded that, in the Kurami Group, (iv) NE–SW axial tension stress was exerted during folding, and (v) ENE–WSW compression strike-slip faulting stress acted after folding.

Stresses (i) and (iv), exerted before 15 Ma, differ from those in the backarc region, suggesting different driving forces between the forearc and backarc regions. Stress (ii), exerted after 15 Ma, differs from that in the near-trench region. Therefore, stress variation in the forearc region can be recorded in the geologic time scale. Stress change would be caused in the Tanabe Group by the trenchward retreat of the northern edge of the near-trench stress domain. Such a stress change is explainable by the occurrence of the dynamic backstop, such as out-of-sequence thrust, at the Tanabe Group's southern border.

This study showed the unique stress in the middle Miocene southwest Japan forearc

region. Furthermore, such stress variation may be detected in other forearc regions, possibly giving new suggestions on subduction-related tectonics.

要旨

現世の前弧域では，プレート沈み込みに伴う変形や物性の空間変化を反映して，応力が空間的に変化する．しかし，このような応力の空間変化が地質構造の違いとして記録され，過去の地質帯からも検出され得るかは議論されてこなかった．西南日本弧には複数の中新世前弧海盆堆積物が分布しており，地質時代の前弧域における応力の空間的非一様性を検討するのに適している．また近年,「西南日本弧全体で 15 Ma 頃に伸張場から南北短縮場に変化した」という従来の描像に反するデータが報告されている．これらのデータは弧内で応力が時空間変化することを示唆するが，前弧域の応力に関する報告は限られている．そのため，当時のテクトニクスを議論する上でも，同時代の前弧域の応力解明が期待される．そこで本研究は，中期中新世の西南日本前弧域における応力の時空間変化を解明する．

本研究では，紀伊半島南西部に分布する下部–中部中新統田辺層群で，1124 枚の砕屑岩脈，402 枚の方解石脈，426 条の小断層を測定し，古応力解析を行った．検出された応力を階層的クラスタリングに基づいて分類することで，以下の 3 つの応力を推定した．(i) 16–15 Ma 頃に働いた，東西方向の最小圧縮主応力軸を持つ応力．(ii) 15 Ma 以降に働いた，北西–南東方向の最大水平圧縮応力軸を持つ応力．(iii) 15 Ma より後に田辺層群南部でのみ働いた，北西–南東引張の正断層型応力．また，静岡県中部に分布する下部中新統倉真層群では，229 条の小断層を測定・解析した．さらに小断層の傾動補正により，16 Ma 頃の褶曲形成との時間関係を検討した．この結果，(iv) 褶曲形成中に北東–南西方向の軸性引張応力が，(v) 褶曲形成後に東北東–西南西圧縮の横ずれ断層型応力が働いたことが分かった．

田辺層群および倉真層群で推定された 15 Ma より前の応力 (i), (iv) はいずれも，背弧域で報告されている応力と異なっている．これは，当時の前弧域と背弧域におけるテクトニクスの駆動力が異なっていたことを示唆する．また，田辺層群で推定された 15 Ma 以降の応力 (ii) は海溝近傍の応力と異なっている．これは前弧域の空間的に非一様な応力が，地質学的時間スケールにおいても記録され得ることを示唆する．田辺層群で 15 Ma 頃に応力が変化したのは，沈み込みに伴う海溝近傍の応力領域が海溝側へ後退したためであると考えられる．このような応力変化は，田辺層群南縁に序列外断層のような動的バックストップが形成されたとすれば説明できる．

このように，中期中新世の西南日本前弧域では，前弧域の空間的に非一様な応力が記録されていた．他の地域・時代の前弧域においても，空間的に非一様な応力が記録されている可能性があり，沈み込み帯のテクトニクスに関する新たな示唆を与えると

期待される.

Table of Contents

1 Introduction

1.1 Non-uniform stress in subduction zones

Revealing crustal stress and its transition is fundamental for understanding the mechanism and driving force of tectonics. Stress in the subduction zone reflects subduction-related forces such as slab-induced dragging or pushing (perpendicular to the subduction interface) and shear force driven by the subduction plate (along the interface) besides mantle drag force acting on the base of the upper plate (Balázs et al., 2022). When only interaction between the subducting plate and the upper plate determines the upper plate stress, the island arc suffers spatially uniform tension or compression (Chemenda et al., 2000). However, taking mantle drag force into consideration, backarc extension or shortening possibly occur independently of forearc shortening (Schellart and Moresi, 2013). Therefore, when discussing stress in the island arc, it is necessary to consider the spatial change of stress.

Especially in the forearc region, spatial variations in stress may be more complicated. Previous studies have proposed the following features producing strain and stress variations or discontinuities in the forearc region. One of the most significant and common structures is the difference in physical properties. "Backstop" (Fig. 1), defined as a region with increased yielding strength compared to the region trenchward, plays a fundamental role in the evolution of forearc geometry (Dahlen, 1990). The continental arc basement possibly acts as a kinematic discontinuity and is called a "static" backstop (Kopp and Kukowski, 2003). A corresponding stress shadow occurs over the backstop, allowing a forearc basin with no or minor deformation (Byrne et al., 1993; Tsuji et al., 2015). As the accretionary wedge grows, differences in physical property occur between the trenchward outer wedge, the actively deforming accretionary wedge, and the landward inner wedge, slowly deforming material resulting from an earlier accretion (Kopp and Kukowski, 2003). Such a relatively consolidated landward region performs as a "dynamic" backstop. For example, an out-of-sequence thrust branching upward from the subduction fault (Park et al., 2002) exists along the Nankai subduction zone where the Philippines Sea Plate is submerged beneath the southwest Japan arc. The thrust is located under the outer arc high bounding inner and outer wedges and is regarded as the dynamic backstop. Besides, strike-slip faults parallel to the trench are known in the obliquely subducting margins (Martin et al., 2010; Mosher et al., 2008). These faults are regarded as the strain partitioning structure

taking the part of the trench-parallel component of obliquely subduction-related displacement, in contrast to the actively deforming outer wedge suffering the trench-perpendicular compression. Such an outline of the deformation structures is controlled by spatial variations in the seismogenic behavior of a subduction fault (Wang and Hu, 2006; Wallace et al., 2012), and the balance of accretion and tectonic erosion (Noda, 2016). Additionally, the seamount subduction influences local deformation and stress (Dominguez et al., 2000). In this way, in the present forearc region, stress varies spatially by subduction-related deformations and spatial variation of physical properties. Even in the paleo-forearc region, spatial non-uniformities of stress might have existed and would suggest the large-scale deformation structures associated with subduction-related tectonics.

Even if stress varied spatially in the paleo-forearc region, we might not detect such spatial non-uniformities of stress for the following two reasons. First, deformation structures form only when the conditions meet their requirement. For example, fault forms when stress meets the Mohr-Coulomb yield criterion. Insufficient differential stress results in no-fault formation. If the stress in the paleo-forearc region did not satisfy the forming requirements of every deformation structure, it would be not recorded as a deformation structure. Second, stress changes temporally. Stresses detected in present forearc regions were derived mainly from geophysical data such as the focal-mechanism solutions of earthquakes and borehole breakout. They reflect stress on the time scales of 10^0–10^2 years. Such stress may not keep working over the geologic time scale, usually 10^5 years or longer, and may not result in enough deformation structures to be detected. In order to verify such possibilities, it is valuable to give an example of spatial non-uniformity of stress in the paleo-forearc region.

1.2 Early to middle Miocene stresses

In southwest Japan, there are early to middle Miocene forearc basin deposits (Fig. 2). It is possible to compare stresses detected in not only a certain basin but separate basins, and they are appropriate for investigating spatial non-uniformity of stress. Conventionally, 15 Ma has been regarded as the tectonic turning point of southwest Japan based on nearly simultaneous episodes such as massive igneous activities (Kimura et al., 2005), formation of unconformity or decrease of sedimentation rate (Nakajima, 2018), and changing stress (Yamamoto, 1991). On the other hand, Hoshi et al. (2015) recently revised the timing of the Japan Sea opening. Instead of kinematic models proposed in the mid-1980s that southwest

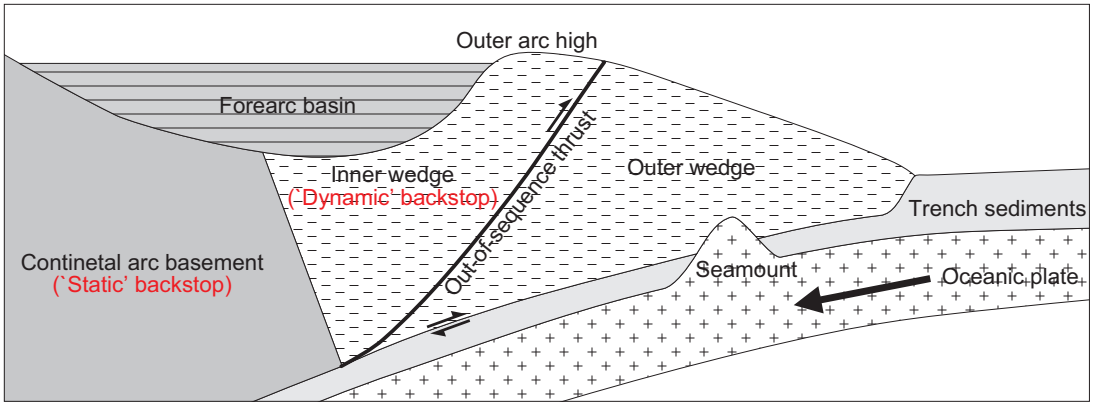

Fig. 1: Schematic diagram of cross section of forearc region.

Japan rotated clockwise on approximately 15 Ma in a short period (Otofuji et al., 1985), southwest Japan mainly rotated clockwise between 17.5 and 15.8 Ma (Hoshi et al., 2015). Therefore, we should check the simultaneity of the episodes.

Details of stress through the early to middle Miocene is also doubtful. Previous studies have revealed stresses acting in the early to middle Miocene in many regions in southwest Japan (Fig. 3 and Table 1). Stress had been considered to change from arc-perpendicular tension to N-S compression all over southwest Japan at 15 Ma simultaneously (e.g., Yamamoto, 1991). Recent studies, however, reported results inconsistent with the above interpretation from the following three viewpoints. First, in the backarc Hokutan Group, normal faulting stress continued after 15 Ma (Haji and Yamaji, 2021) incongruously with the above interpretation. Second, recent studies are revising intrusion ages of igneous dikes used for the maximum horizontal stress (σ_{Hmax}) direction estimation. Contrary to previous estimations, parts of E-W striking igneous dikes have intruded after 15 Ma (Tatsumi et al., 2001; Sato and Haji, 2021). Third, in the forearc region, no igneous dike before 15 Ma has been reported, and the stress before 15 Ma is not estimated. Therefore, it is significant to reveal the stress in the early to middle Miocene forearc region from also the viewpoint of tectonics.

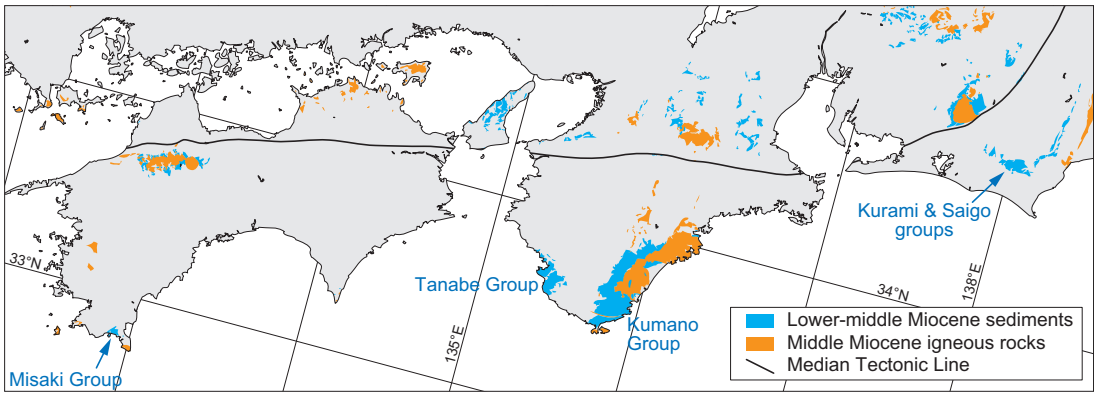

Fig. 2: Map of southwest Japan based on the 1:200,000 scale Seamless Geological Map of Japan [URL1]. 'Lower-middle Miocene sediments' include volcaniclastic rocks.

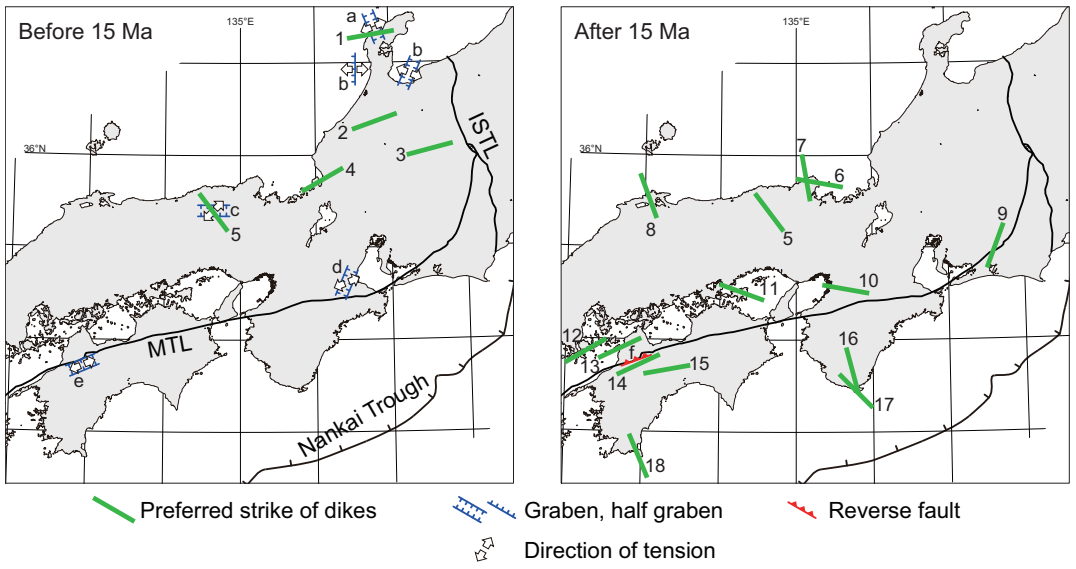

Fig. 3: Stress orientation and map-scale deformation structures in southwest Japan before and after 15 Ma. Details of dike swarms are shown in Table 1. The references for map-scale structures are a: Kobayashi et al. (2005); b: Nakajima et al. (2021); c: Haji and Yamaji (2020); d: Kinoshita and Yamaji (2021); e: Kusuhashi and Yamaji (2001); f: Takeshita (1993).

Table 1: Preferred strikes and age of dike swarms reported previously. Uncertainties of the age obtained from a sample are only shown. Abbreviations: FT (fission track), Pen. (Peninsula).

No	Place name	Trend	Age (Ma)	Method	Reference
1	Wajima	80	ca. 16	Stratigraphically	Kobayashi (1979), Yamamoto (1991), Yanagisawa (1999)
2	Hakusan	70	ca. 17–16	Stratigraphically	Ishiwatari and Ohama (1997), Kobayashi (1979)
3	Takane	67.5	17.66 ± 0.33	Whole rock K–Ar	Sugisaki and Hoshi (2017), Tanase et al. (2001)
4	Tsuruga	67.5	18.99–18.94	Whole rock K–Ar	Hoshi and Takagawa (2009), Sato et al. (2013)
5	Tajima	45	17.1–13.7	Zircon U–Pb	Haji and Yamaji (2021)
6	Tango	-80	ca. 15	Stratigraphically	Yamamoto and Hoshizumi (1988)
7	Tango	-10	14.5–12.6	Whole rock K–Ar	Yamamoto (1991), Yamamoto and Hoshizumi (1988)
8	Sakaiminato	-20	ca. 14	Stratigraphically	Kano and Yoshida (1985)
9	Shitara	20	16.5–14.9	Whole rock K–Ar	Takada (1988), Tsubakawa et al. (1983)
10	Shigisan	-80	ca. 15.0–14.5	Stratigraphically	Hoshi et al. (2002), Tatsumi et al. (2001)
11	Shodo-Shima	-70	13.4–12.4	Whole rock K–Ar	Tatsumi et al. (2001)
12	Yashirojima	45	12.1 ± 0.1	Zircon U–Pb	Sato and Haji (2021)
13	Matsuyama	65	12.6–12.4	Zircon U–Pb	Shinjoe et al. (2017), Tatsumi et al. (2001)
14	Kuma	65	14.5–14.4	Zircon U–Pb	Shinjoe et al. (2017), Yamaji and Sato (2011)
15	Takaiwa	80	15.0 ± 0.5	Whole rock K–Ar	Kobayashi (1979), Umehara et al. (1991)
16	Muro	-22.5	14.4–13.9	Zircon FT	Haji et al. (2022)
17	Shionomisaki	-45	14.6 ± 0.2	Zircon U–Pb	Haji et al. (2022), Shinjoe et al. (2019)
18	Ashizuri	-22.5	13.1–13.0	Zircon U–Pb	Murakami et al. (1989), Shinjoe et al. (2010)

1.3 Objective of this study

In order to reveal spatial variation (or uniformity) in the middle Miocene forearc region in southwest Japan, this study applied the stress inversion method to outcrop-scale deformation structures. Except for the Kumano Group, no study reveals paleo-stress history recorded in lower-middle Miocene forearc basin deposits. As a target for constructing stress history, the Tanabe Group, distributed in the southwestern Kii Peninsula, has the following advantages. First, various outcrop-scale deformation structures can be observed: clastic dikes, mineral veins, and outcrop-scale faults. Each structure is formed under different conditions. Fluid inject into the existing joint and clastic dikes and mineral veins form if fluid pressure exceeds the normal stress applied to the joint. They do not require large differential stress to be formed, unlike fault. On the other hand, faults are formed when meeting the failure condition and do not require fluid supply. Because of such differences, analyzing various deformation structures enable us to detect heterogeneous stresses. It is an advantage for revealing the spatial and temporal variation of stress. Second, we can compare detected stresses to that reported in other areas in the Kii Peninsula. In the Kumano Group, some studies have measured outcrop-scale deformation structures and applied the stress inversion method to them (Choi et al., 2011; Miura, 2005; Otsubo et al., 2009; Yamanaka, 2016; Yamanaka and Yamaji, 2017). In addition, some igneous activity, such as Kumano Acidic Rocks and Shionomisaki Igneous Complex, occurred in the middle Miocene, and some igneous dikes associated with them have been used to estimate stress (Haji et al., 2022; Miura, 2005). Stresses in the Tanabe Group can be compared to the stresses in other areas in the Kii Peninsula to consider several tens-of-kilometers-scale uniformity of stresses.

Therefore, this study reveals paleo-stress in the Tanabe Group by applying the stress inversion method to structural data. Additionally, this study reveals paleo-stress in the Kurami Group in the easternmost southwest Japan to consider along-arc variation (or uniformity) of stresses.

2 Geological setting

2.1 Southwest Japan

The southwest Japan arc has the belt-like distribution of some geological zones. The Median Tectonic Line divides southwest Japan into continental Inner and trenchward Outer zones, respectively. Outer Zone is subdivided into Sanbagawa Metamorphic Complex, Chichibu Supergroup, and Shimanto Supergroup. Shimanto Supergroup is the accretionary complex formed between Cretaceous and Miocene.

In southwest Japan, many Miocene sedimentary basins are distributed, including forearc basins such as the Kurami, the Saigo, the Kumano, the Tanabe, and the Misaki groups (Fig. 2). The depositional ages of the base of each forearc basin are constrained by the foraminifers between Blow's (1969) N6 and N8 (Tanabe Research Group, 1984; Kimura, 1985; Shiba et al., 2020). Foraminifers indicating the depositional age as the N8 zone have been reported in many of the basins (Saito, 1960; Nishimura and Miyake, 1973; Ikebe et al., 1975; Tanabe Research Group, 1984; Ibaraki, 1986; Shiba et al., 2020) except for the Misaki Group. On the other hand, foraminifers of the N9 zone have been reported only from the Kumano Group (Ikebe et al., 1975). Therefore, the upper limit of the depositional ages is suggested indirectly to be around 15 Ma (Ozaki, 2009; Takano, 2017), the boundary between Blow's (1969) N8 and N9 (15.12 Ma; Raffi et al., 2020).

2.2 The Tanabe Group

The Tanabe Group (Fig. 4) is distributed in southwestern part of the Kii Peninsula. The Tanabe Group is divided into the lower Asso and upper Shirahama formations (Fig. 5). The Asso Formation is subdivided into the Iwayadani, Maro, Hisogawa, and Gohchidani members in ascending order and is composed mainly of conglomerate and mudstone. The Shirahama Formation is subdivided into the S1-S5 members in ascending order and mainly consists of sandstone, alternations of sandstone and mudstone, and conglomerate. Toshima conglomerate beds overlies the Shirahama Formation unconformably. In addition, clastic dikes and intruding mudstone with conglomerates regarded as mud diapir widely occur in the Tanabe Group (Shimizu, 1985).

Synclines with gentle westward-plunging axes characterize the overall Tanabe Group. Besides, bedding undulates by E–W trending fold axes, although dipping angles of bedding

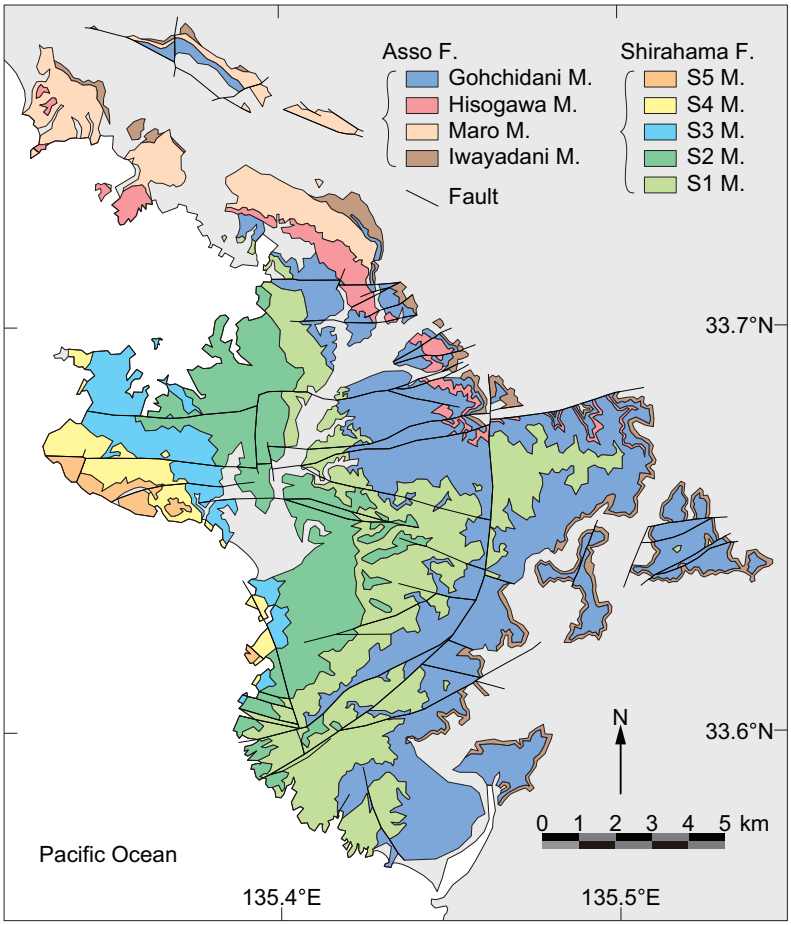

Fig. 4: Geological map of the Tanabe Group (after Tanabe Research Group, 1992). Abbreviations: F. (Formation) and M. (Member).

are generally less than 20°. E–W and N–S trending map-scale faults are indicated, but most parts of them are unknown in their detailed attitudes and faulting directions and senses.

Tanabe Research Group (1984) reported foraminifers from the Gohchidani Member, the Asso Formation, and correlated the occurrence horizon to Blow's (1969) N8 zone. Especially, *Praeorbulina Glomerosa* was included, and the Gohchidani Member can be correlated to Wade et al.'s (2011) M5b zone (16.3–15.1 Ma; Raffi et al., 2020).

2.3 The Kurami and the Saigo groups

The Kurami and the Saigo groups (Fig. 6) are distributed in the central part of Shizuoka Prefecture. The Kurami Group overlies the Mikura and Setogawa groups unconformably

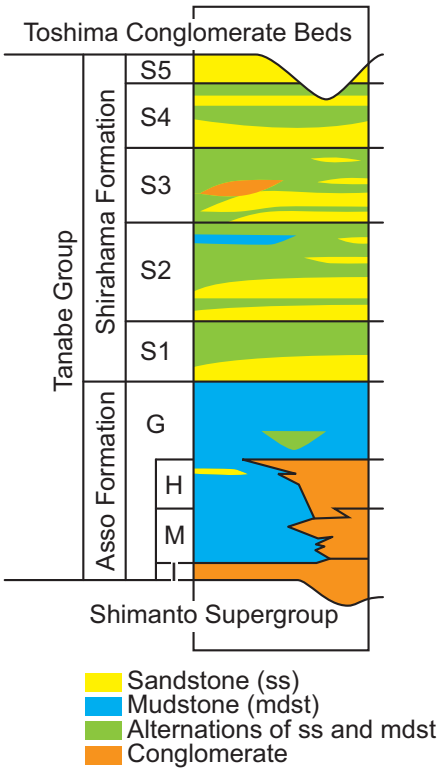

Fig. 5: Schematic columnar section of the Tanabe Group (after Tanabe Research Group, 1992). Member abbreviations: G (Gohchidani), H (Hisogawa), M (Maro), and I (Iwayadani).

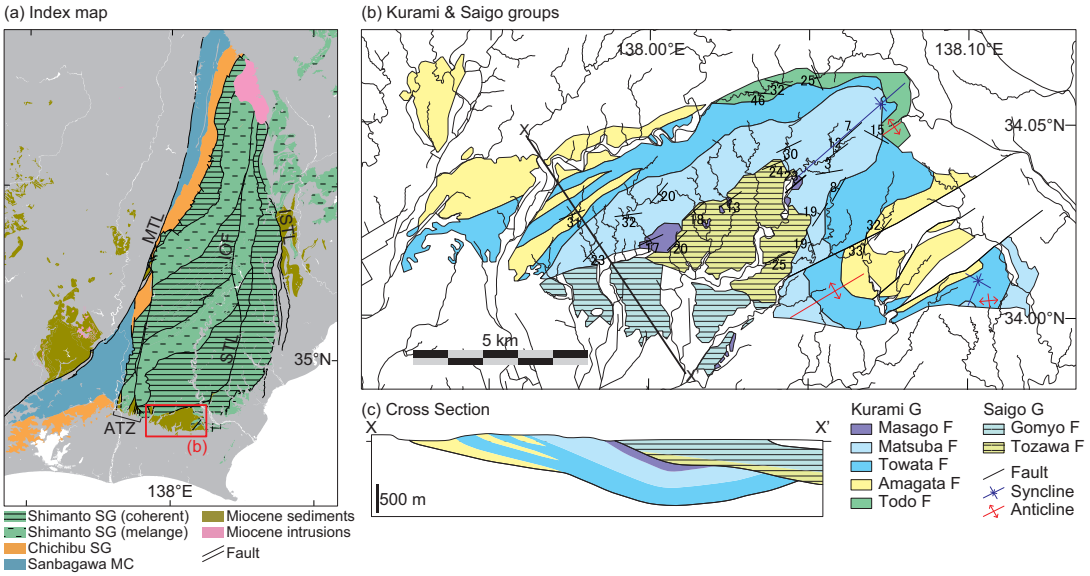

Fig. 6: (a) Index map, (b) a geological map of the Kurami and Saigo groups, and (c) their cross-section. (a) is based on the 1:200,000 scale Seamless Geological Map of Japan [URL1], and (b, c) are after Shiba et al. (2020). The location of (c) is shown as X–X' in (b). Abbreviations in (a): IOF (Ikawa-Okaramatsuyama Fault), ISTL (Itoigawa-Shizuoka Tectonic Line), MC (Metamorphic complex), MTL (Median Tectonic Line), and SG (Supergroup). Abbreviations in legends: F (Formation), and M (Member).

(Shiba et al., 2020). The Kurami Group is divided into the Todo, the Amagata, the Towata, the Matsuba, and the Masago formations in ascending order. The Saigo Group overlies the Kurami Group unconformably. The Saigo Group is divided into the Tozawa and the Gomyo formations in ascending order.

NE–SW trending folds characterize the Kurami Group. On the other hand, the Saigo Group shows south to southeastward monoclinal structure and is not folded (Fig. 6c). It indicates that the folding in the Kurami Group had occurred before the Saigo Group deposited.

Some studies reported foraminifers from the Kurami and the Saigo groups (Saito, 1960; Ibaraki, 1986; Shiba et al., 2020). They correlated the depositional ages of the Kurami Group to Blow's (1969) N6–N8 zones and the Saigo Group to the N8 zone. Yoshimura et al. (1989) determined the fission track ages of zircon from tuff layers. Determined ages from the Towata Formation are 17.08±0.97 and 17.80±1.05 Ma, and that from the Matsuba Formation is 17.94 ± 0.84 Ma.

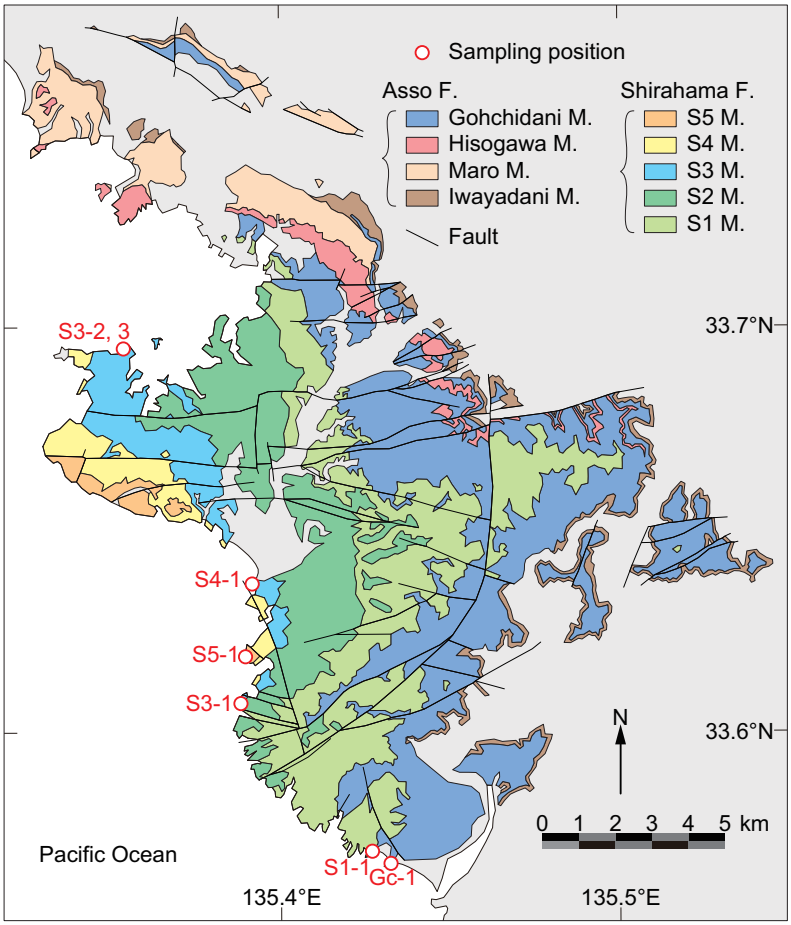

Fig. 7: Map of sampling positions for zircon U–Pb dating in the Tanabe Group. The geological map is after Tanabe Research Group (1992). Abbreviations: F. (Formation) and M. (Member).

3 Constraints on the depositional age of the Tanabe Group

Although there are some detailed constraints on the depositional age of the Asso Formation, the upper limit of the depositional age of the Shirahama Formation is uncertain. In order to constrain the depositional age of the Tanabe Group, this study determined the U–Pb ages of detrital zircons extracted from the Shirahama and the uppermost Asso formations. Sampling positions and stratigraphic horizons are summarized in Fig. 7 and Table 2.

Table 2: Sampling positions and stratigraphic horizons for detrital zircon U–Pb dating.

Name	Longitude	Latitude	Member (Formation)
Gc-1	135°25′56.4″E	33°34′4.2″N	Gohchidani (Asso)
S1-1	135°25′37.1″E	33°34′16.0″N	S1 (Shirahama)
S3-1	135°23′17.6″E	33°36′28.0″N	S3 (Shirahama)
S5-1	135°23′23.4″E	33°37′7.0″N	S5 (Shirahama)
S4-1	135°23′29.8″E	33°38′11.9″N	S4 (Shirahama)
S3-2	135°21′16.0″E	33°41′40.8″N	S3 (Shirahama)
S3-3	135°21′16.0″E	33°41′40.8″N	S3 (Shirahama)

3.1 Method

Mounts of zircons were separated and polished following Haji et al. (2019). Cathodoluminescence and back scattered electron (BSE) images were taken using an electron-probe micro-analyzer (EPMA: JEOL JXA-8105) equipped with Hamamatsu Photonics high voltage power supply C9525 and photon counting unit C9744 at Kyoto University to check the presence of zonal structures, cracks, and inclusions.

U–Pb analyses were conducted using the LA-ICP-MS system installed in the Geochemical Research Center, Graduate School of Science, the University of Tokyo. This system consists of a femtosecond laser-ablation instrument (Jupiter Solid Nebulizer, St Japan Inc.) and a multi-collector inductively-coupled-plasma mass spectrometry instrument (MC-ICP-MS: Nu Plasma II, Nu Instruments Ltd.). The measurement settings of the instruments are given in Table 3. Following isotopes are measured; ^{202}Hg, ^{204}Pb + Hg, ^{206}Pb, ^{207}Pb, ^{208}Pb, ^{232}Th and ^{235}U. Numbers of ^{238}U count were calculated from those of ^{235}U using ^{238}U/^{235}U = 137.88. ^{207}Pb/^{206}Pb was normalized by analyses of the NIST SRM 612 (^{207}Pb/^{206}Pb = 0.90726; Jochum et al., 2005), and ^{206}Pb/^{238}U by the Nancy 91500 zircons (^{206}Pb/^{238}U = 0.17917; Wiedenbeck et al., 1995) or the GJ-1 zircons (^{206}Pb/^{238}U = 0.09761; Jackson et al., 2004). The OD-3 zircons (^{206}Pb–^{238}U age: 33.0 ± 0.1 Ma; Iwano et al., 2013) were used as secondary standard materials for age quality control. Analysis spots were determined based on surface structures of polishing and cathodoluminescence images. Possible Pb contamination of zircon surfaces was eliminated by pre-cleaning with single-shot laser ablation (Iizuka and Hirata, 2004). Errors of isotope ratios and ages were determined using counting statistical errors and repeatability of ^{206}Pb/^{238}U of the Nancy

Table 3: LA-ICP-MS instruments and operational conditions.

Femtosecond Laser ablation system	
Instrument	Jupiter Solid Nebulizer (ST Japan Inc., Tokyo, Japan)
Laser wavelength	260 nm
Fluence	3 J cm^{-2}
Repetition rate	1000 Hz
Ablation duration	1 s
Ablation pit size	20 μm
Carrier gas	He and Ar make-up gas combined outside ablation cell
He gas flow rate	0.6 L/min
Ar make-up gas flow rate	0.6 L/min (for samples S3-1, S3-2, S3-3) or 0.8 L/min (for samples Gc-1, S1-1, S5-1, S4-1)
ICP-MS instrument (MC-ICP-MS)	
Instrument	Nu Plasma II (Nu Instruments Ltd., Wrexham, U.K.)
Sample introduction	Ablation aerosol
RF power	1300 W
Detection system	Mixed Faraday-multiple ion counting array
Monitored isotopes	^{202}Hg, ^{204}Pb+^{204}Hg, ^{206}Pb, ^{207}Pb, ^{208}Pb, ^{232}Th, ^{235}U
Detector	Three Daly detectors (^{206}Pb, ^{207}Pb, ^{235}U), three secondary electron multipliers (^{208}Pb, ^{204}(Hg+Pb), ^{202}Hg), and single Faraday cup (^{232}Th)

91500 or the GJ-1 zircons and ^{207}Pb/^{206}Pb of the NIST SRM 612 analyzed before and after sample analyses. Analysis values of $90 < 100 \times (^{238}\text{U}\text{–}^{206}\text{Pb age}/^{235}\text{U}\text{–}^{207}\text{Pb age}) < 110$ were regarded as concordant data (e.g., Zhang et al., 2016). Note that this study ignores the effects of common Pb and initial disequilibria caused by intermediate nuclides in the ^{238}U and ^{235}U decay series (e.g., Wendt and Carl, 1985).

3.2 Result

Results are shown in Fig. 8 as the Concordia diagrams (Wetherill, 1956), the probability density distribution plots (Hurford et al., 1984), and the histograms. In this subsection, ^{238}U–^{206}Pb ages are used for zircons younger than 1000 Ma, and ^{207}Pb–^{206}Pb ages are applied for the zircons older than 1000 Ma. Uncertainties of the ages indicate twice of

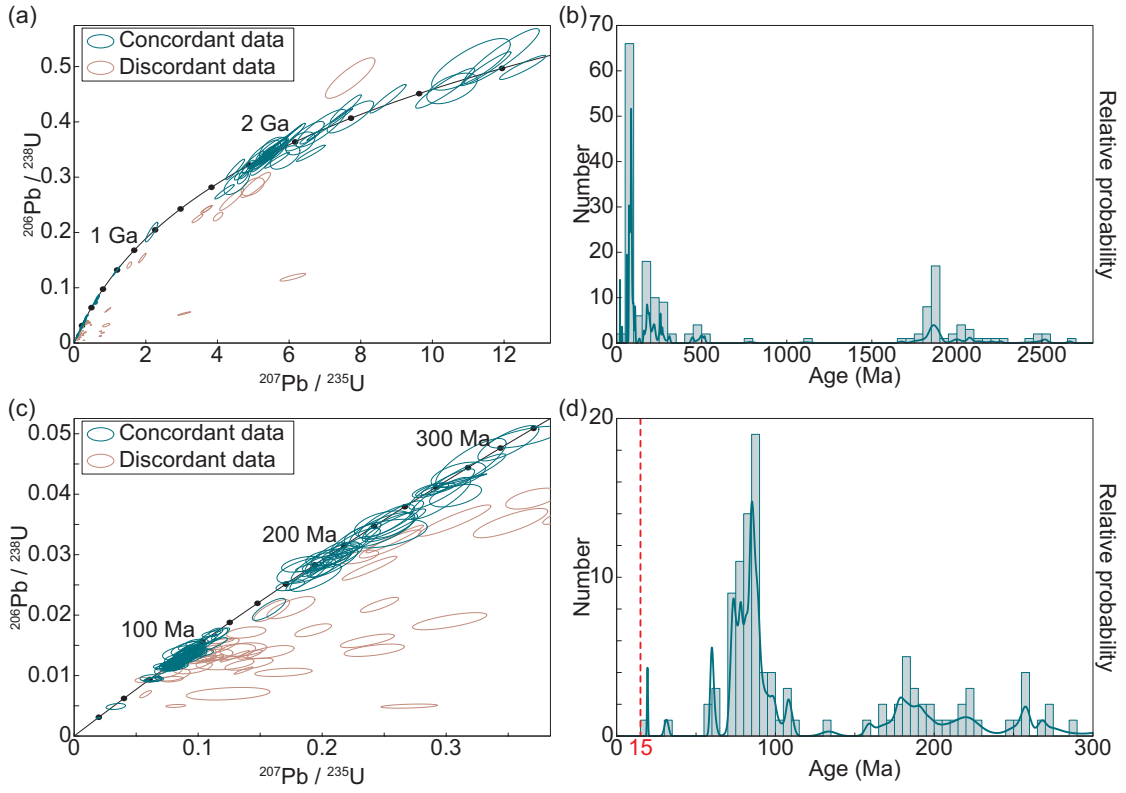

Fig. 8: Analysis results of detrital zircons. (a, c) Concordia diagrams. (b, d) Histograms and probability density plots. (b, c) Results of all data and (c, d) data younger than 300 Ma. Data-point error ellipses in concordia diagrams are 2σ.

standard deviations (2σ). OD-3 zircons analyzed as the secondary standard showed 32.8 ± 0.2 Ma. This age is consistent with the reference age (33.0 ± 0.1 Ma; Iwano et al., 2013) within the 2σ error range. 235 zircon grains were analyzed, and 174 concordant ages were obtained. The youngest age of the samples was 19.4 ± 0.6 Ma.

In southwest Japan, many igneous activities occurred after 15 Ma, such as near-trench magmatism, outer-zone igneous activities, Setouchi volcanic activities, and others (Fig. 9). If the deposition of the Shirahama Formation continued after 15 Ma, the formation should include materials younger than 15 Ma. No analyzed zircon grain is younger than 15 Ma, and this study concludes that the depositional age of the Tanabe Group is older than 15 Ma.

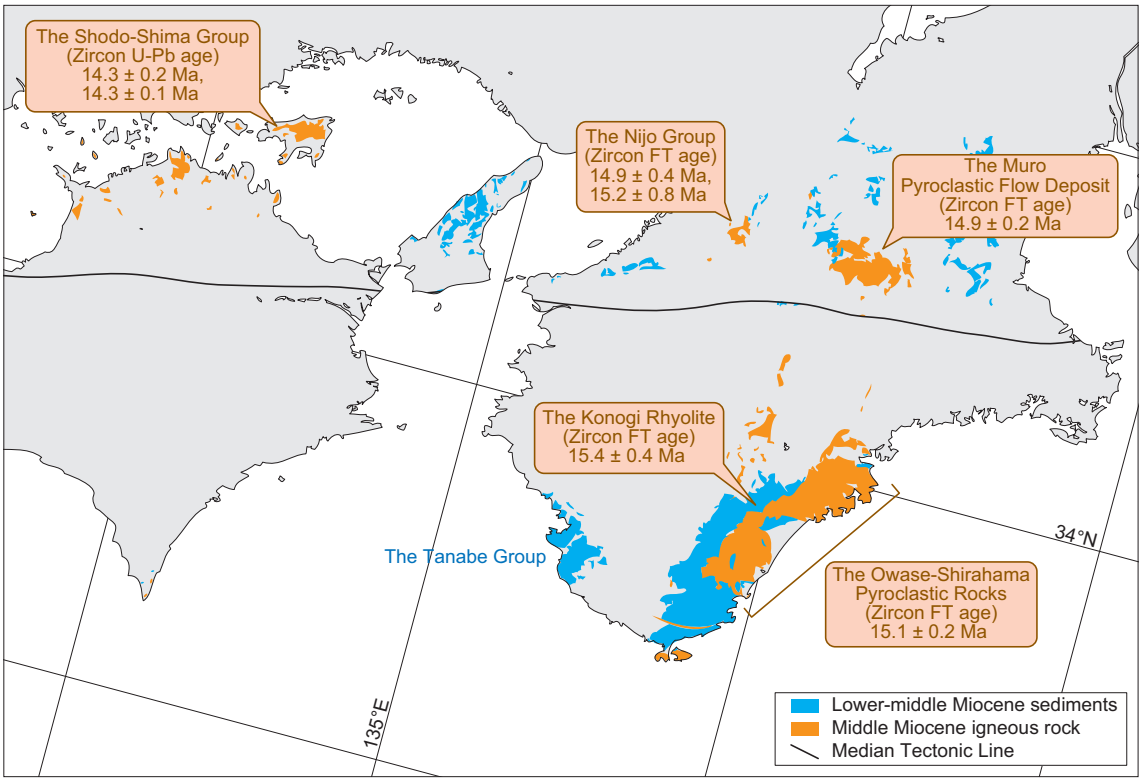

Fig. 9: Ages of volcaniclastic rocks around the Kinki district. The references for them are the Shodo-Shima Group: Tatsumi et al. (2010); the others: Iwano et al. (2007). Distributions of sediments and igneous rocks are based on the 1:200,000 scale Seamless Geological Map of Japan [URL1]. 'Lower-middle Miocene sediments' include volcaniclastic rocks. Abbreviation: FT (fission track).

4 Stress inversion

4.1 Outcrop-scale deformation structures

This study observed clastic dikes, mineral veins, and outcrop-scale faults.

Many clastic dikes intrude the Tanabe Group. They mainly consist of mudstone (Fig. 10a), although some sandstone dikes exist (Fig. 10b). Pebbly mudstone intrusions treated as mud diapirs (Fig. 10c, d) also exist in the Tanabe Group (Shimizu, 1985). Some clastic dike swarms were supplied from the mud diapirs (Miyata et al., 2009). Typically, clastic dikes intrude related to seismic activity (Cho et al., 2017), rapid loading (Hildebrandt and Egenhoff, 2007), and sediment mobilization (Davies et al., 2006). In the Kumano basin offshore the Kii Peninsula, some mud volcanoes exist. They were formed by excessive fluid supplied from the basement accretionary wedge or the deeper subducting fault (Asada et al., 2021). Mud diapirs and surrounding clastic dikes in the Tanabe Group may also have such an origin.

Mineral veins were observed in the Tanabe and Kurami groups (Fig. 11a). Those in the Tanabe Group only comprise calcite, whereas those in the Kurami Group consist of quartz and calcite. In the Tanabe Group, some veins crosscut calcareous concretions (Fig. 11b). They do not inject into the host rock, suggesting that these veins were formed during or after the concretion formation. Generally, many calcareous concretions are centered on fossils and formed soon after their mortem (Yoshida et al., 2015). If the concretion growth occurred in the early stage of compaction, surrounding laminas should bend because of the difference in consolidation degree between in and out of the concretion (Marshall and Pirrie, 2013). In the Tanabe Group, however, laminas around the concretions do not bend (Fig. 11c, d), suggesting that the concretions and the veins were formed after compaction. The mineralization in the Tanabe Group may have been influenced by the activity of Karekinada arcuate dikes (Harada and Nakaya, 1999). In the Kurami Group, some veins have fault-related characteristics, such as en echelon array (Fig. 11e, f) and shear veins. They can form under local stress instead of regional stress, and they cannot be distinguished from the veins unrelated to faults. Thus, this study did not analyze veins in the Kurami Group.

This study also measured fault-slip data of outcrop-scale faults. Fault-slip data include the attitude of the fault plane, slip direction (Fig. 12a) and slip sense (Fig. 12b). Some faults have all the information and are called “full data” (Sato, 2006). Some, however, have

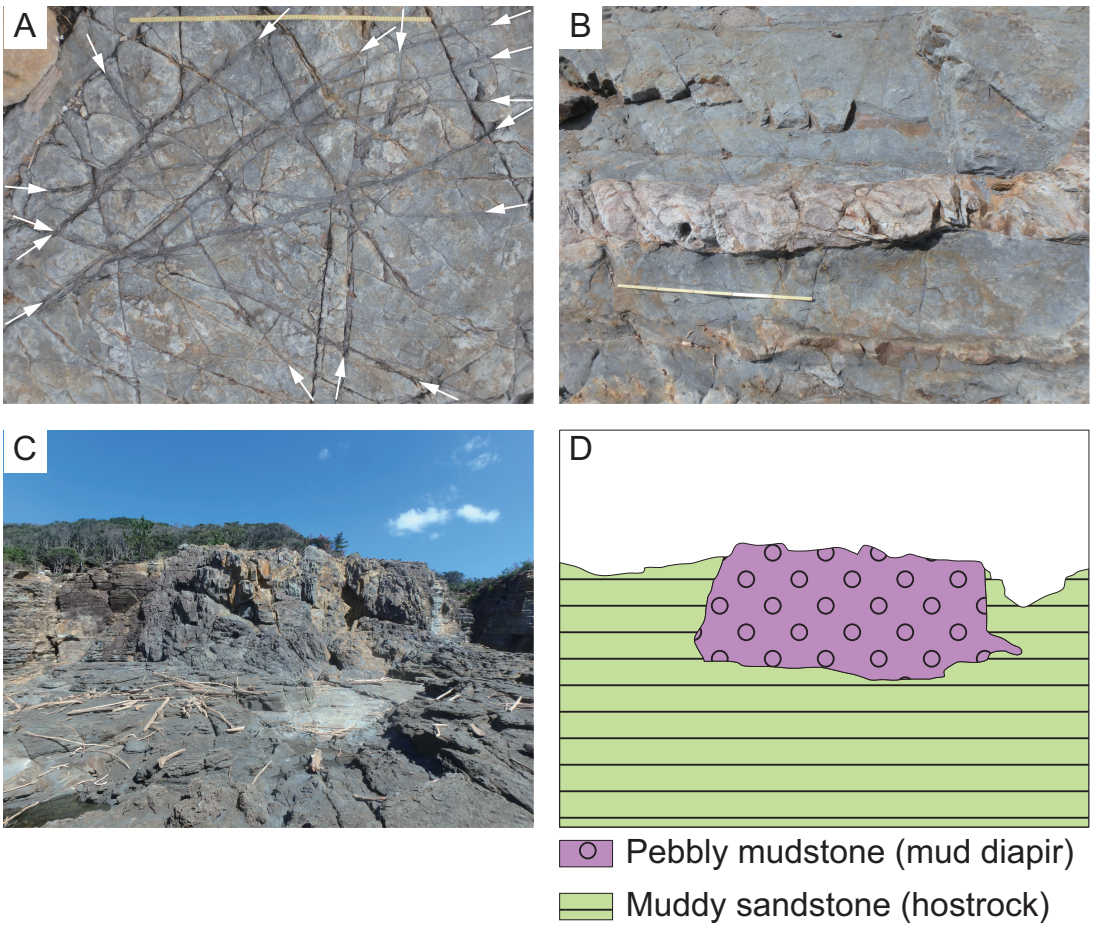

Fig. 10: Photographs of (a) mud dikes (indicated by arrows), (b) a sand dike, and (c) a mud diapir. (d) The associated sketch diagram of (c) is also shown. Note the 1 m scales in (a) and (b). The diapir in (c) is 15 m wide.

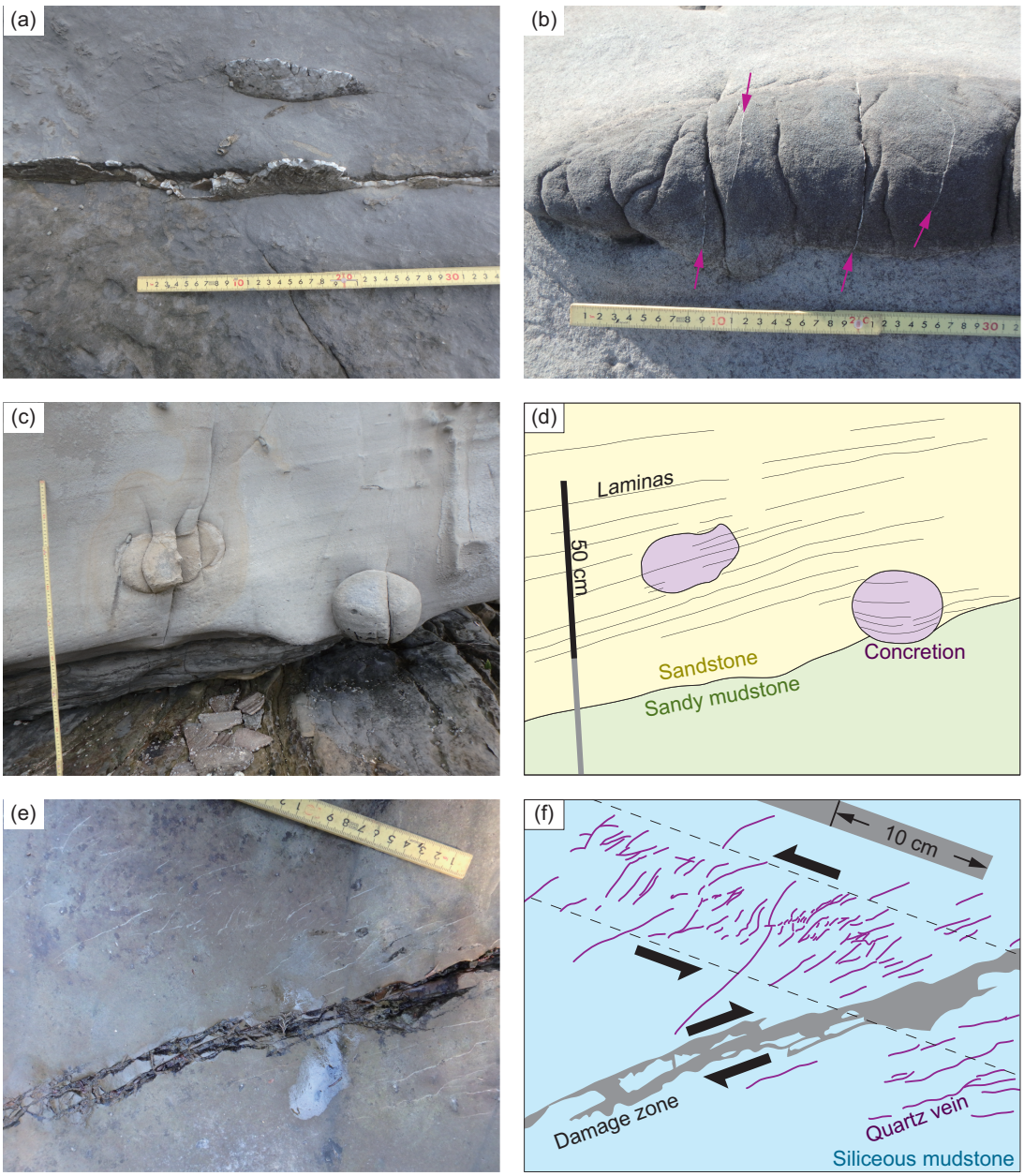

Fig. 11: Photographs of (a) a calcite vein, (b) a calcareous concretion with calcite veins (indicated by arrows), and (c) calcareous concretion with laminas in the Tanabe Group, (e) quartz veins of en echelon array in the Kurami Group. (d, f) The associated sketches of (c) and (e), respectively.

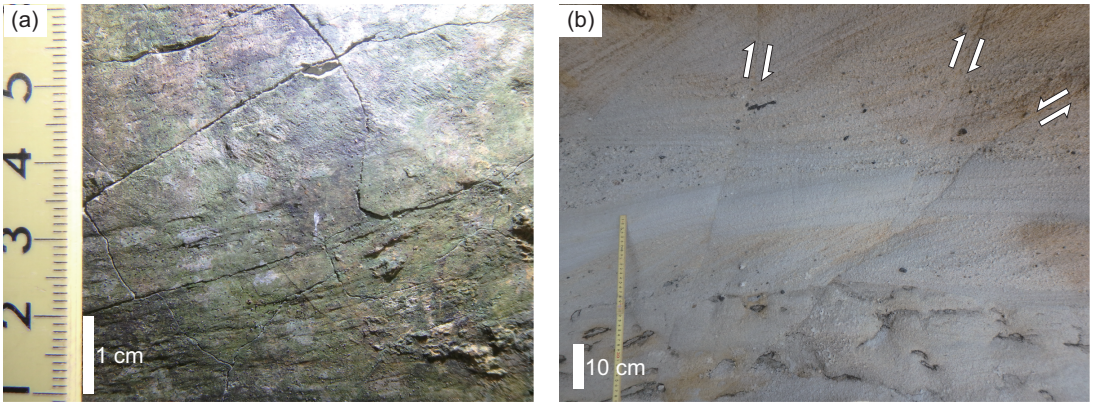

Fig. 12: Photographs of faults with apparent (a) slip directions and (b) slip senses. In (a), striations falling to the right are observed in the upper half, and subhorizontal striations are seen in the lower half.

neither slip direction nor sense, called "sense-only" and "line-only" data, respectively.

4.2 Stress inversion methods

This study treats compression as positive stress. The principal stresses satisfy $\sigma_3 \leq \sigma_2 \leq \sigma_1$. The stress ratio is defined as $\phi = (\sigma_2 - \sigma_3)/(\sigma_1 - \sigma_3)$ (Baer et al., 1994). The following methods give us "a state of stress," referring, in this study, to the stress collectively that have the principal orientation and stress ratio in common.

To clastic dikes and mineral veins, this study applied the "mixed Bingham distribution method" (Yamaji and Sato, 2011). Dike intrusion and vein injection occur when fluid pressure exceeds normal stress on the joint (Delaney et al., 1986). Dikes and veins are easy to intrude perpendicularly to the minimum principal stress σ_3 axis and are hard to intrude perpendicularly to the maximum principal stress σ_1 axis. As a result, poles of dikes or veins under tectonic stress show anisotropic distribution. Yamaji et al. (2010) showed that the distribution could be approximated by the Bingham distribution (Bingham, 1974). Poles of dikes or veins intruding under heterogeneous stresses distribute as the sum of weighted Bingham distributions (Yamaji and Sato, 2011). These weighting coefficients are called the mixing coefficient. This method returns mixing coefficients besides states of stress. Additionally, this method calculates the membership, indicating ease of explanation of each dike for each detected stress. High membership suggests easy explanation.

Table 4: Data numbers of the structures in each areas in the Tanabe Group.

Area	Clastic dikes	Mineral veins	Outcrop-scale faults
A	-	-	31
B	119	62	-
C	-	19	-
D	-	117	-
E	-	-	35
F	64	30	51
G	96	27	27
H	-	52	101
I	869	19	85
J	-	76	96
total	1148	402	426

For outcrop-scale faults, the "Hough transform inverse method" (Sato, 2006) was employed. The slip direction is assumed to be parallel to the shear stress (Wallace, 1951; Bott, 1959). Based on this hypothesis, more appropriate stress should reduce the misfit angle d, defined as the difference between observed slip directions and shear stress. The fitness function is the monotonically decreasing function for d. The Hough transform inverse method calculates the goodness of fit, defined as the sum of the fitness function, for each predetermined stress. In this situation, optimum stress has the largest goodness of fit. As a result, this study shows the states of stress with a relatively large goodness of fit.

4.3 The Tanabe Group

Structural data were measured in 10 areas in the Tanabe Group (Fig. 13 and Table 4) to estimate paleo-stress. This section reports data and results of stress analyses for each structure: clastic dikes, mineral veins, and outcrop-scale faults.

4.3.1 Clastic dikes

In 4 areas, 1148 clastic dikes in total were measured.

Analysis results in areas B, F, and G are shown in Fig. 14. In Area B, 119 clastic dikes were measured, and strike-slip faulting stress with E–W σ_3 axis and moderate ϕ (defined as

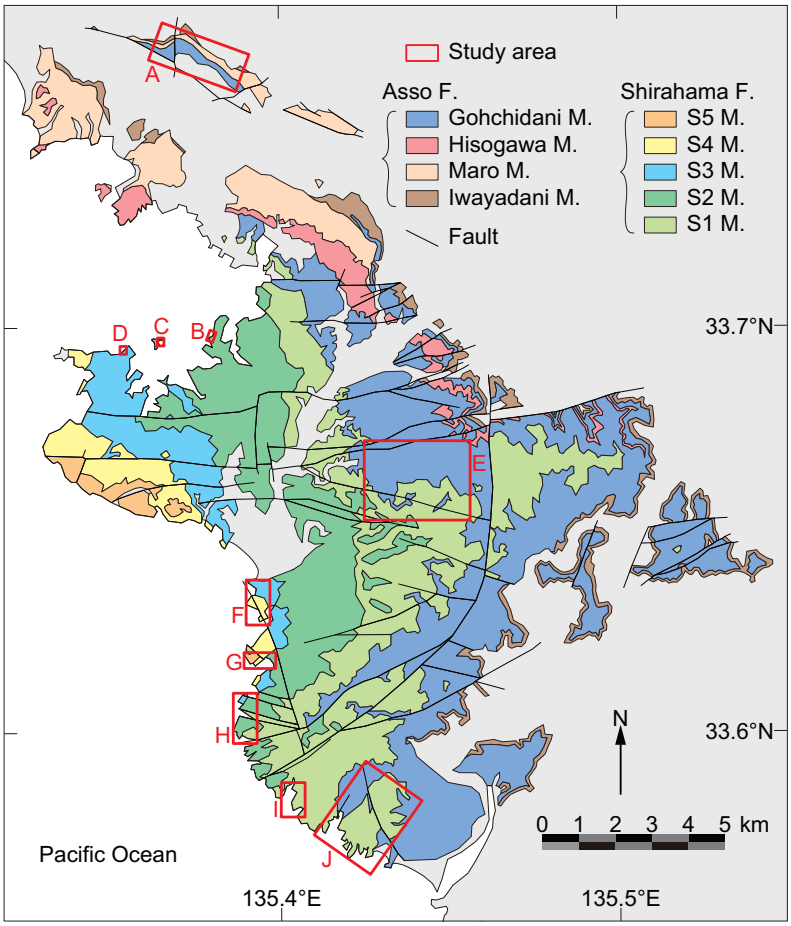

Fig. 13: An index map of the study areas in the Tanabe Group. The geological map is after Tanabe Research Group (1992). Abbreviations: F. (Formation) and M. (Member).

Stress Bd-α) was detected (Fig. 14a). In Area F, 64 clastic dikes were measured, and two stresses were detected (Fig. 14b): σ_1-plunging stress with NE–SW σ_3 axis and moderate ϕ (Stress Fd-α), and normal faulting stress with E–W σ_3 axis and small ϕ (Stress Fd-β). In Area G, 96 clastic dikes were measured, and two stresses were detected (Fig. 14c): σ_1-plunging stress with E–W σ_3 axis and large ϕ (Stress Gd-α), and σ_1-plunging stress with WNW–ESE σ_3 axis and moderate ϕ (Stress Gd-β).

In Area I, 845 mud dikes and 24 sand dikes were measured. Some mud diapirs were recognized in this area, and their intrusions may have induced local and episodic changes in stress states. After analyses, normal faulting stress with WNW–ESE σ_3 axis (Stress Id-α) was detected from mud dikes in all sub-areas, suggesting that the stress was regional and had a tectonic origin (Abe and Sato, 2021). From sand dikes, normal faulting stress with NNW–SSE σ_3 axis and moderate ϕ (Stress Id-β) was detected.

4.3.2 Mineral veins

In 8 areas, 402 mineral veins in total were measured (Fig. 15).

In Area B, 62 veins were measured, and strike-slip faulting stress with NNE–SSW σ_3 axis and large ϕ (Stress Bv-α) was detected (Fig. 15a). In Area C, 19 veins were measured, and two stresses were detected (Fig. 15b): σ_1-plunging stress with NNE–SSW σ_3 axis and moderate ϕ (Stress Cv-α), and σ_1-plunging stress with E–W σ_3 axis and moderate ϕ (Stress Cv-β). This study ignores the latter stress because of the small mixing coefficient of the stress and the small data number in this area. In Area D, 117 veins were measured, and normal faulting stress with ENE–WSW σ_3 axis and moderate ϕ (Stress Dv-α) was detected (Fig. 15c). In Area F, 30 veins were measured, and normal faulting stress with NNE–SSW σ_3 axis and small ϕ (Stress Fv-α) was detected (Fig. 15d). In Area G, 27 veins were measured, and two stresses were detected (Fig. 15e): σ_1-plunging stress with NNE–SSW σ_3 axis and moderate ϕ (Stress Gv-α), and strike-slip faulting stress with E–W σ_3 axis and small ϕ (Stress Gv-β). This study ignores the latter stress because of the small mixing coefficient of the stress. In Area H, 52 veins were measured, and normal faulting stress with NE–SW σ_3 axis and moderate ϕ (Stress Hv-α) was detected (Fig. 15f). In Area I, 19 veins were measured, and two stresses were detected (Fig. 15g): strike-slip faulting stress with NE–SW σ_3 axis and small ϕ (Stress Iv-α), and σ_1-plunging stress with NNW–SSE σ_3 axis and moderate ϕ (Stress Iv-β). This study ignores the latter stress because of

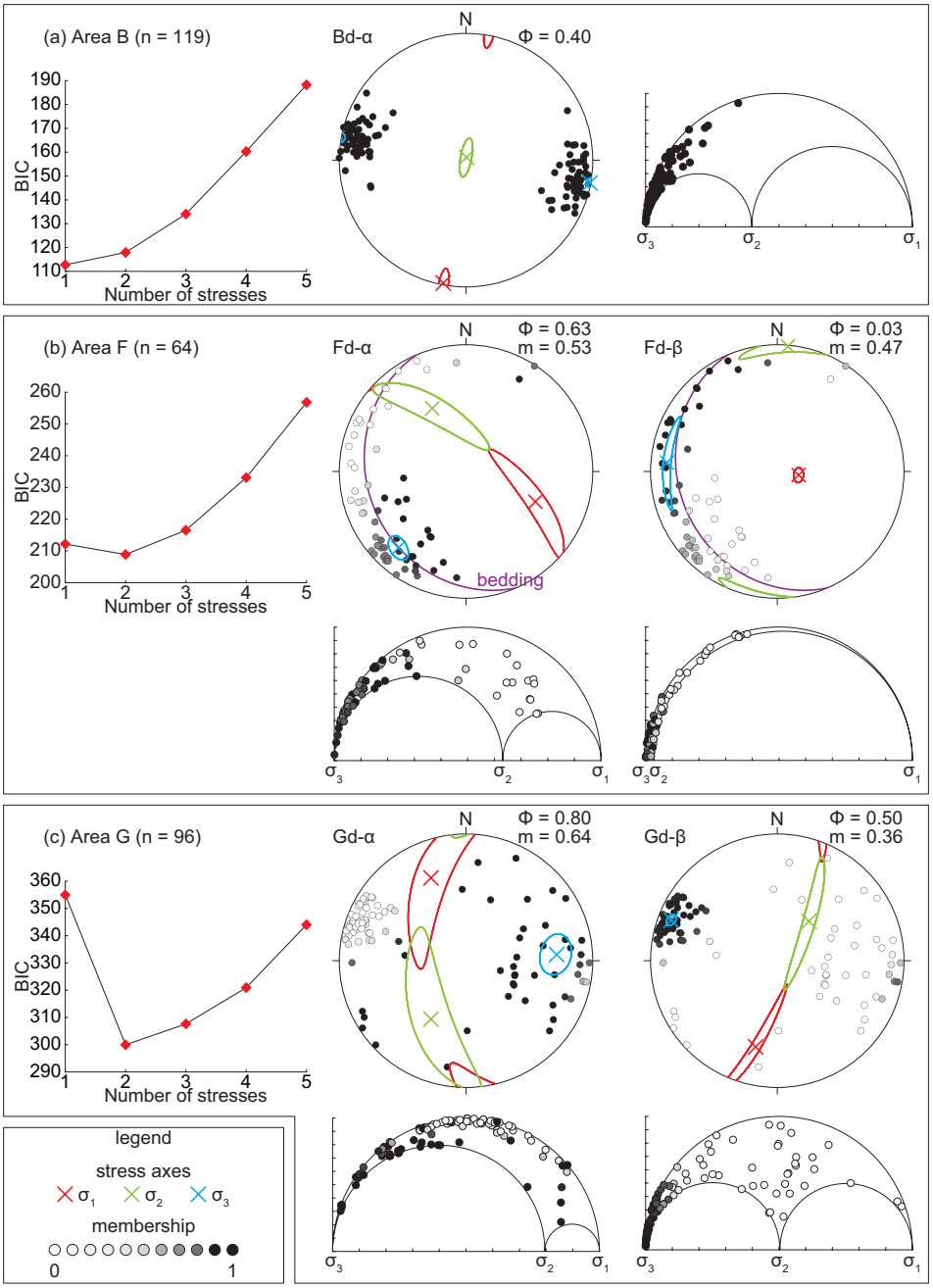

Fig. 14: Paleo-stress analysis of the clastic dike attitudes in Areas B, F, and G in the Tanabe Group. The left graphs in each result plot BIC (Bayesian information criterion) against the number of stresses. On the right, the lower hemisphere equal-area projections show dike orientations and principal stress axes with 95% confidence areas. Semicircles are Mohr's circles of each stress, and dots represent dike planes. The darker color of the dots shows larger membership for the stress. Abbreviations: n (number of data), ϕ (stress ratio), and m (mixing coefficient).

the small mixing coefficient of the stress and the small data number in this area. In Area J, 76 veins were measured, and two stresses were detected (Fig. 15h): normal faulting stress with NNW–SSE σ_3 axis and moderate ϕ (Stress Jv-α), and strike-slip faulting stress with NE–SW σ_3 axis and moderate ϕ (Stress Jv-β).

4.3.3 Outcrop-scale faults

In 7 areas, 426 outcrop-scale faults in total were measured (Fig. 16).

In Area A, 31 faults were measured, and normal faulting stress with NW–SE σ_3 axis and small ϕ (Stress Af-α) was detected (Fig. 16a). Stress Af-α explains 24 data (77% of the whole data). In Area E, 35 faults were measured, and normal faulting stress with WNW–ESE σ_3 axis and large ϕ (Stress Ef-α) was detected (Fig. 16b). Stress Ef-α explains 27 data (77%). In Area F, 51 faults were measured, and normal faulting stress with NE–SW σ_3 axis and moderate ϕ (Stress Ff-α) was detected (Fig. 16c). Stress Ff-α explains 36 data (71%). In Area G, 27 faults were measured, and reverse faulting stress with WNW–ESE σ_1 axis and small ϕ (Stress Gf-α) was detected (Fig. 16d). Stress Gf-α explains 25 data (93%). In Area H, 101 faults were measured, and strike-slip faulting stress with NNE–SSW σ_3 axis and moderate ϕ (Stress Hf-α) was detected (Fig. 16e). Stress Hf-α explains only 69 data (68%). Unexplained 32 data were separately analyzed, and reverse faulting stress with NNW–SSE σ_1 axis and moderate ϕ (Stress Hf-β) was detected. Stresses Hf-α and Hf-β explain 88 data (87%). In Area I, 85 faults were measured, and two stresses were detected (Fig. 16f): normal faulting stress with NNW–SSE σ_3 axis and large ϕ (Stress If-α), and strike-slip faulting stress with NW–SE σ_1 axis and small ϕ (Stress If-β). Stress If-α explains 51 data (60%), while stresses If-α and If-β explain 69 data (81%). In Area J, 96 faults were measured, and normal faulting stress with NW–SE σ_3 axis and moderate ϕ (Stress Jf-α) was detected (Fig. 16g). Stress Jf-α explains only 55 data (57%). Unexplained data were analyzed, and strike-slip faulting stress with NE–SW σ_3 axis and moderate ϕ (Stress Jf-β) was detected. Stresses Jf-α and Jf-β explain 78 data (81%).

4.3.4 Cross-cutting relationships

In order to constrain the order of detected stresses, cross-cutting relationships between the structures were observed (Fig. 17).

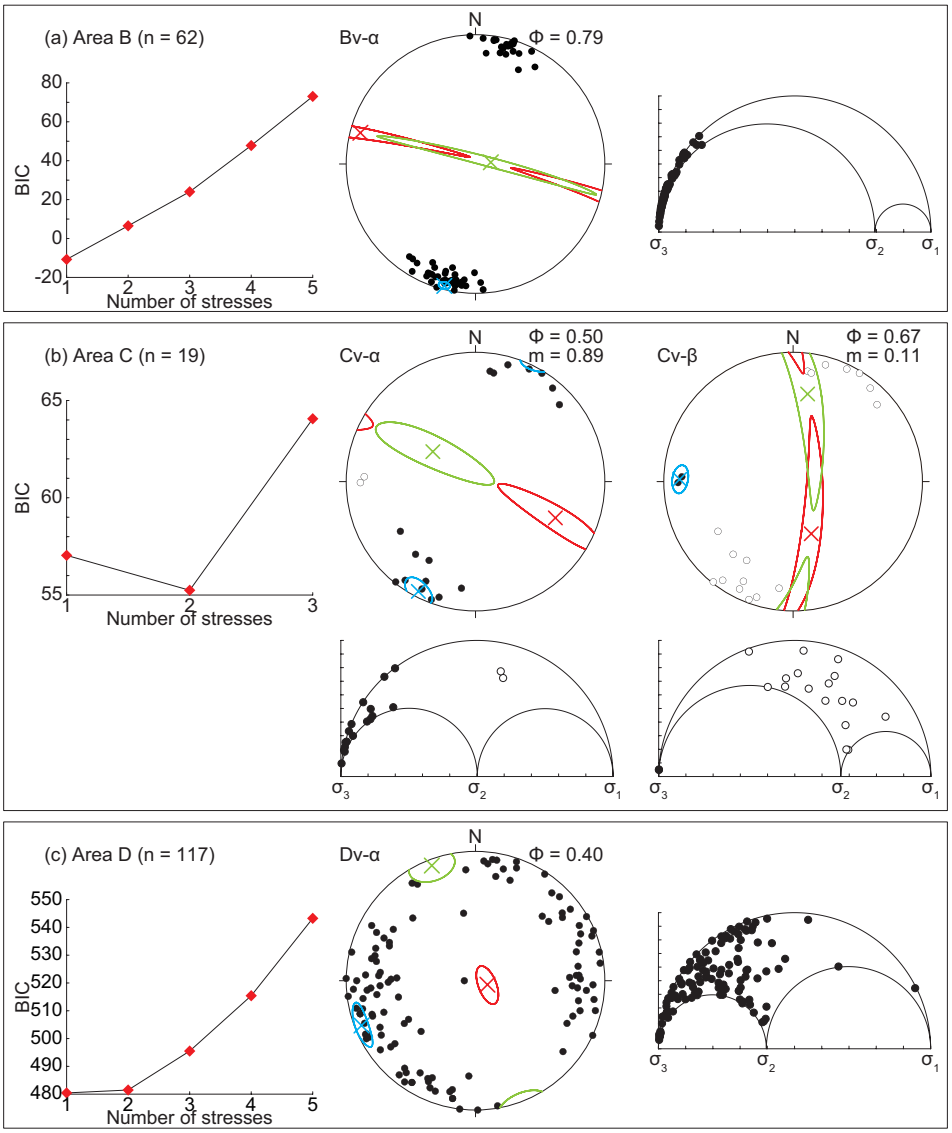

Fig. 15: Paleo-stress analysis of the mineral vein attitudes in areas B, C, D, F, G, H, I, and J in the Tanabe Group. Legends are the same as Fig. 14.

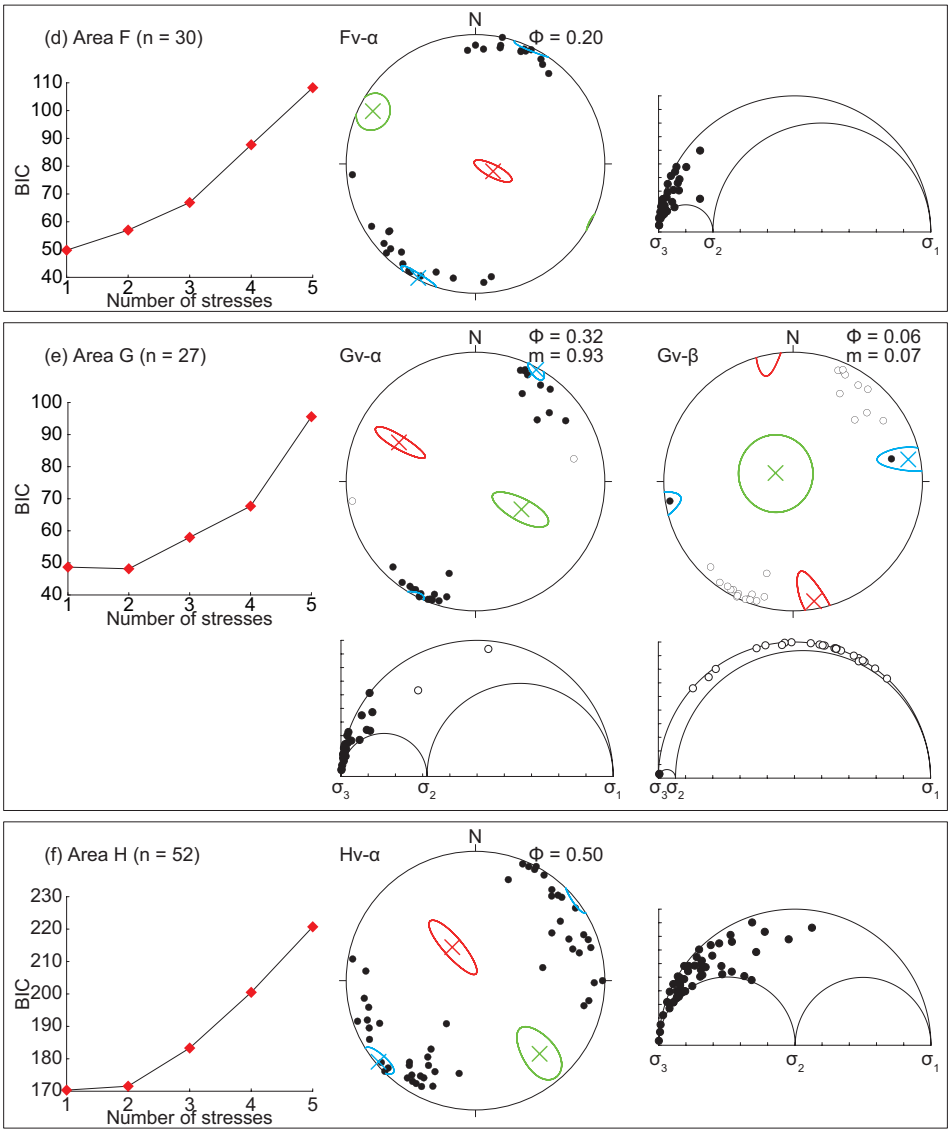

Fig. 15: Continued.

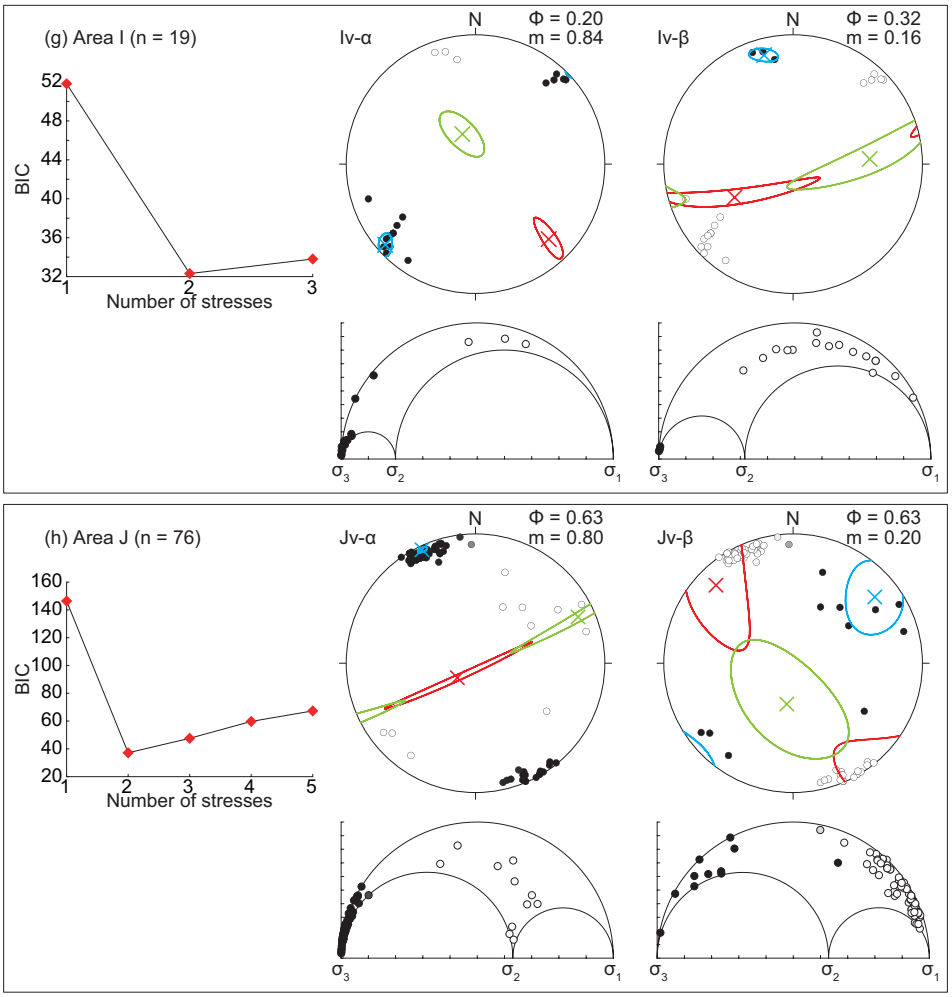

Fig. 15: Continued.

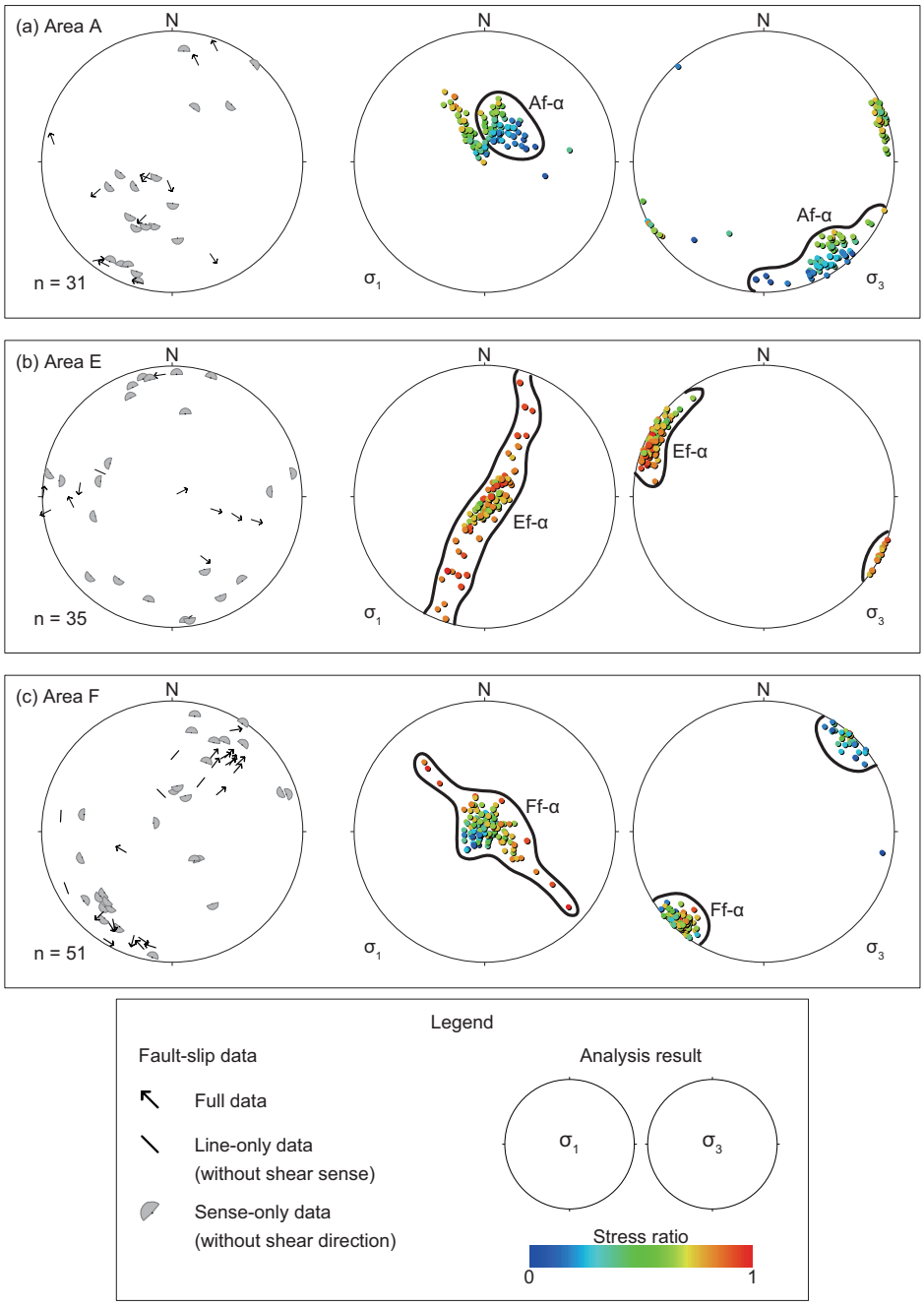

Fig. 16: Outcrop-scale fault-slip data and their paleo-stress analysis results in areas A, E, F, G, H, I, and J in the Tanabe Group. For the data in areas H and J, unexplained data by an optimum stress were reanalyzed.

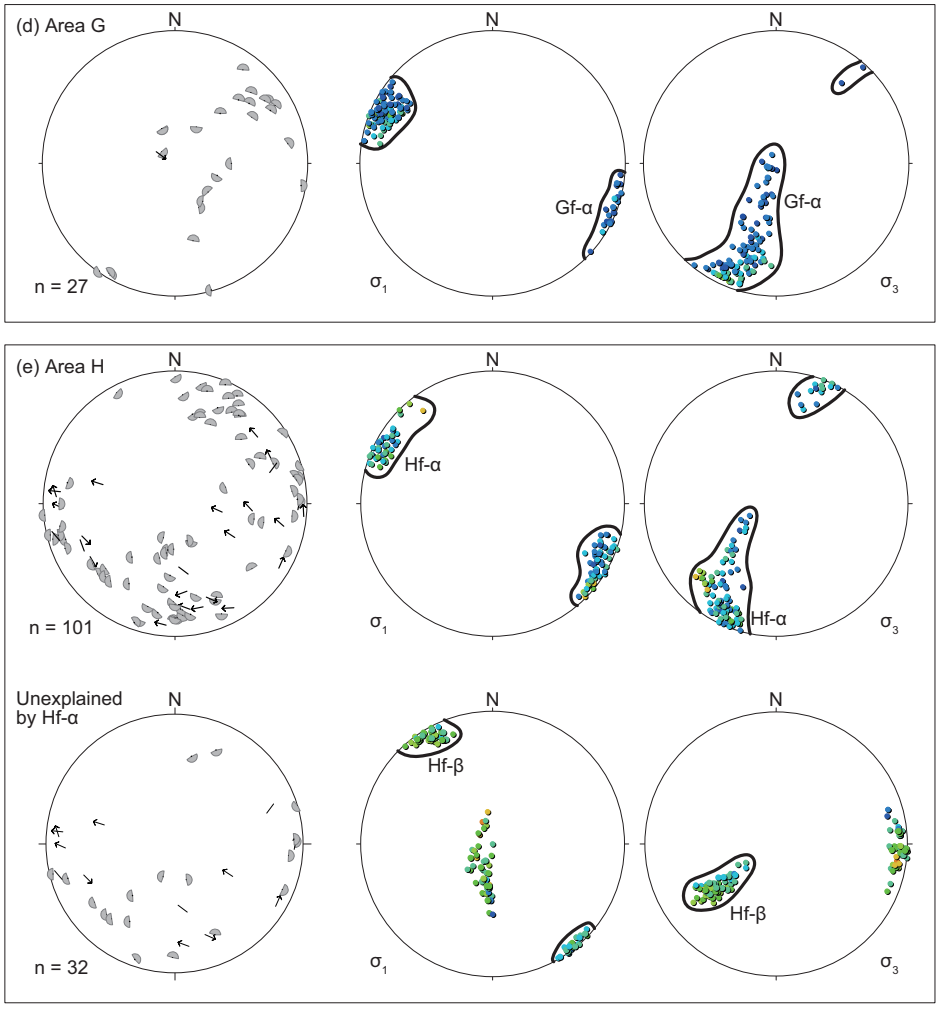

Fig. 16: Continued.

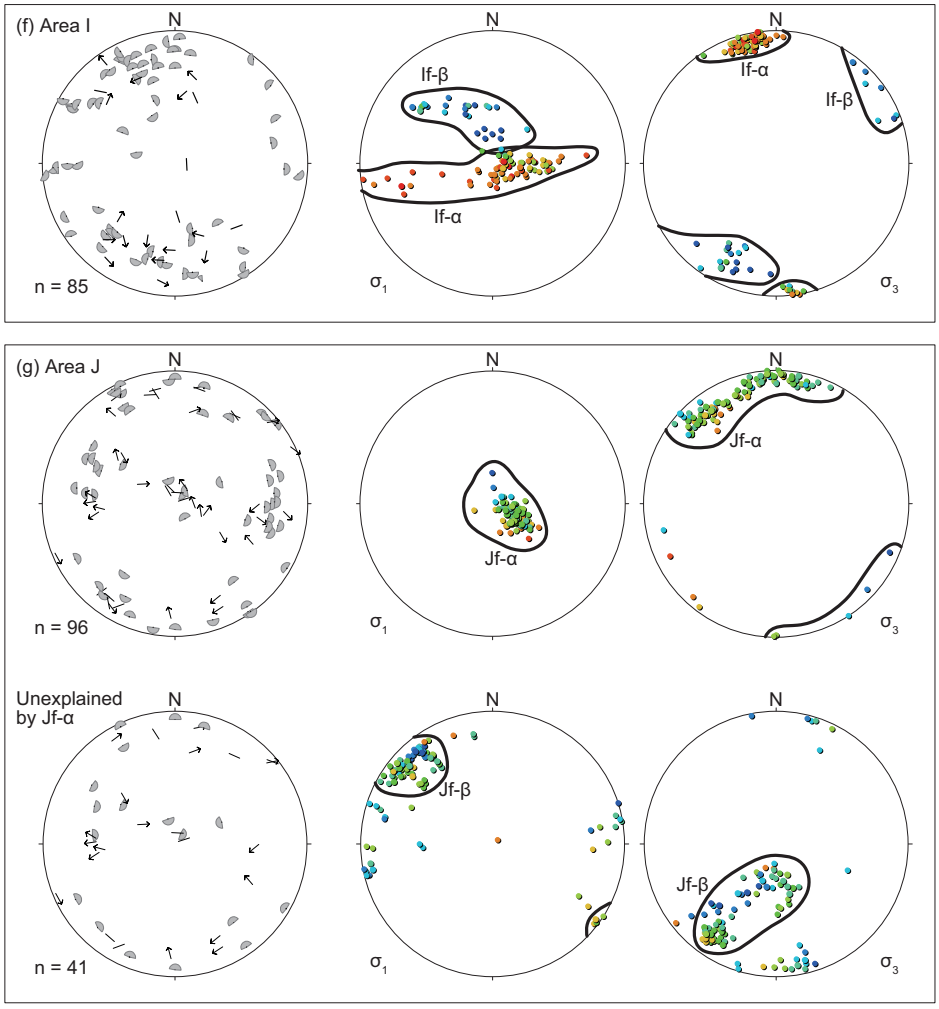

Fig. 16: Continued.

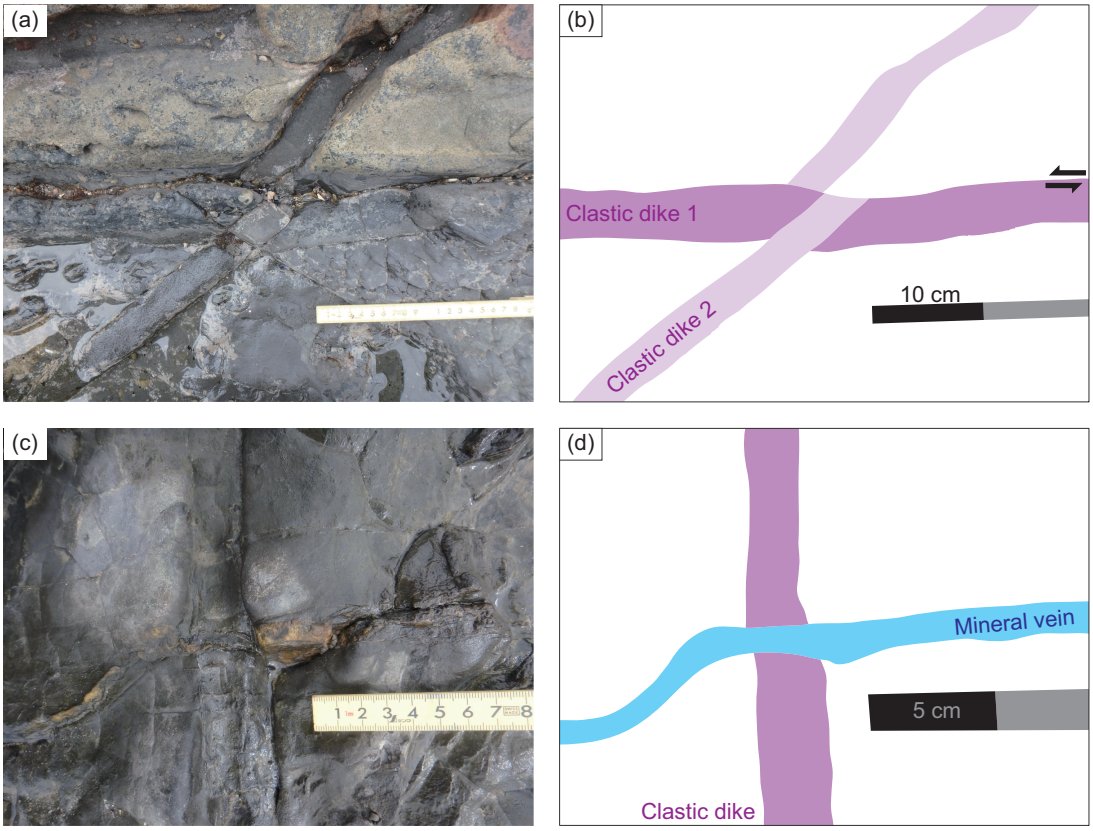

Fig. 17: Photographs of cross-cutting relationships between (a) clastic dikes in Area F, and (c) a clastic dike and a mineral vein in Area G. (b, d) The associated sketches of (a) and (c), respectively. Note that, in (a), Clastic dike 1 had intruded before Clastic dike 2, and then a fault along Clastic dike 1 was activated and displaced Clastic dike 2.

In Area F, 15 cross-cutting relationships between clastic dikes were observed. Memberships for Stress Fd-α were calculated for earlier and later dikes (Fig. 18). For the nine relationships, earlier dikes have small membership for Stress Fd-α (large for Fd-β), and later dikes have large membership for Stress Fd-α. However, no relationship showed a reverse order. Therefore, it was supported that Stress Fd-β preceded Stress Fd-α.

In Area G, all mineral veins cut the clastic dikes, showing that Stress Gd-α or Gd-β worked before Stress Gv-α. In Area I, all mineral veins cut mud dikes, indicating that Stress Id-α worked before Stress Iv-α. Additionally, in Area I, all sandstone dikes cut mud dikes, indicating that Stress Id-α was exerted before Stress Id-β (Abe and Sato, 2021).

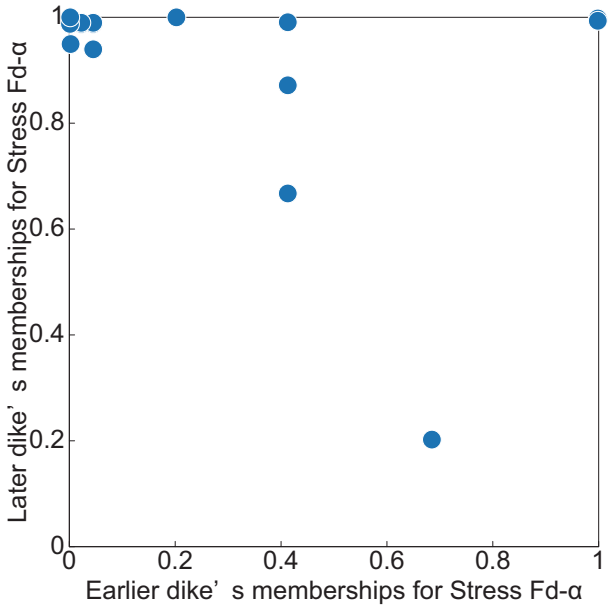

Fig. 18: Memberships of cross-cutting clastic dikes for Stress Fd-α. Memberships of dikes intruding earlier are plotted on the horizontal axis and later are plotted on the vertical axis. Relationships plotted on the upper left side indicate that Stress Fd-α worked after Stress Fd-β, and those on the bottom right indicate reverse order.

4.4 The Kurami Group

In the Kurami Group, 229 outcrop-scale fault data were measured (Fig. 19). By analyzing all data, NE–SW axial tension (large ϕ) stress was detected (Fig. 20a).

The Kurami Group, however, has fold structures, and the detected stress may not be the original stress. Therefore, this study applied tilt correction of the faults to determine the temporal relationship between the stress and folding (Tonai et al., 2011). The bedding near each fault was treated as the reference plane. Faults were rotated on the axis of the strike in stages (every 5%) until the reference bedding became horizontal. At all stages, NE-SW axial tension stress was optimum. The goodness of fit for the optimum stress became largest at 35% of the correction factor (Fig. 20b). This suggests that NE-SW axial tension stress acted during folding. The optimum stress for 35% corrected data is named Stress Kf-α (Fig. 20c). Stress Kf-α explains only 129 tilt-corrected data (56%).

By analyzing unexplained 100 data, strike-slip faulting stress with ENE–WSW σ_1 axis and small ϕ was detected (Fig. 21a). When applying tilt correction to these data, the goodness of fit for the optimum stress became largest at 5% of the correction factor (Fig.

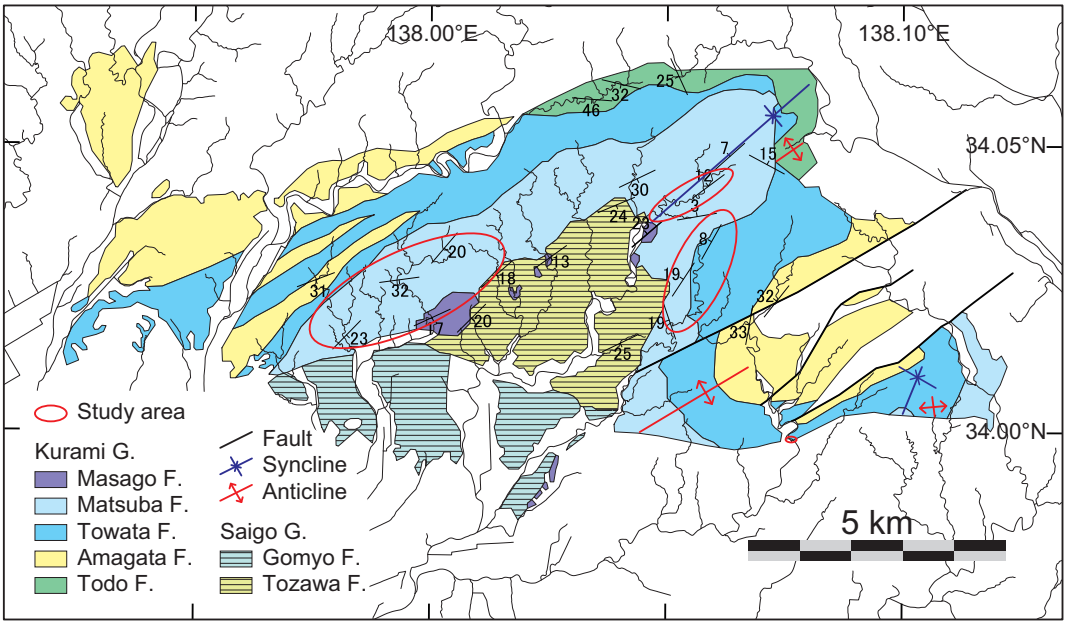

Fig. 19: An index map of the study areas in the Kurami Group. The geological map is after Shiba et al. (2020) Abbreviations: F. (Formation) and M. (Member).

21b). This suggests that ENE-WSW compression strike-slip faulting stress acted at the end of (or perhaps after) folding. The optimum stress for 5% corrected data is named Stress Kf-β (Fig. 21c). Stress Kf-α and Kf-β explain 187 data (82%).

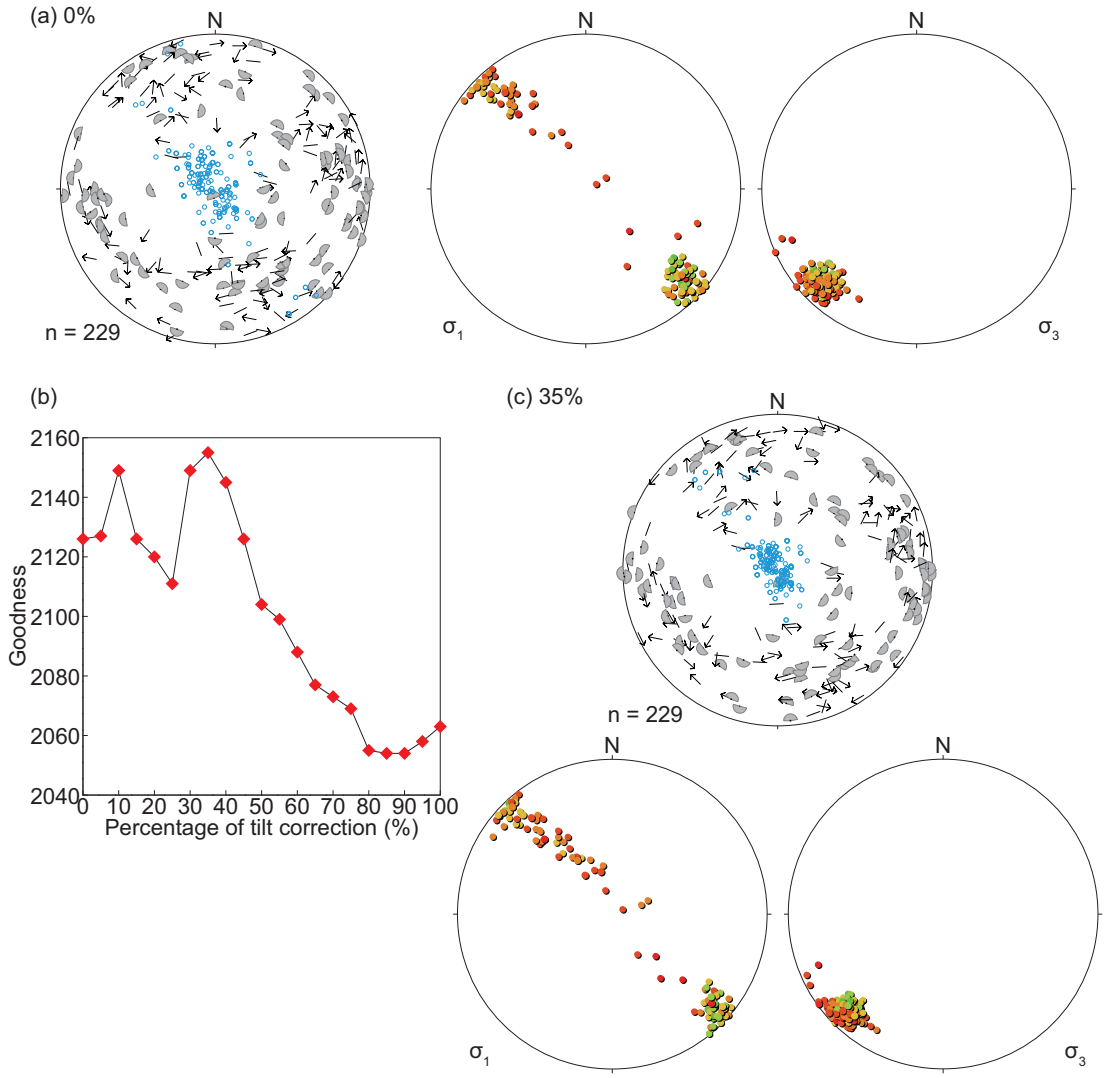

Fig. 20: Outcrop-scale fault data in the Kurami Group and analysis results. (a) data and the analysis result for original attitudes. (b) a plot of goodness for each stage of tilt correction. (c) data and the analysis result after 35% tilt correction. Blue circles in the data stereogram show bedding near the fault. The other legends are the same as Fig. 16.

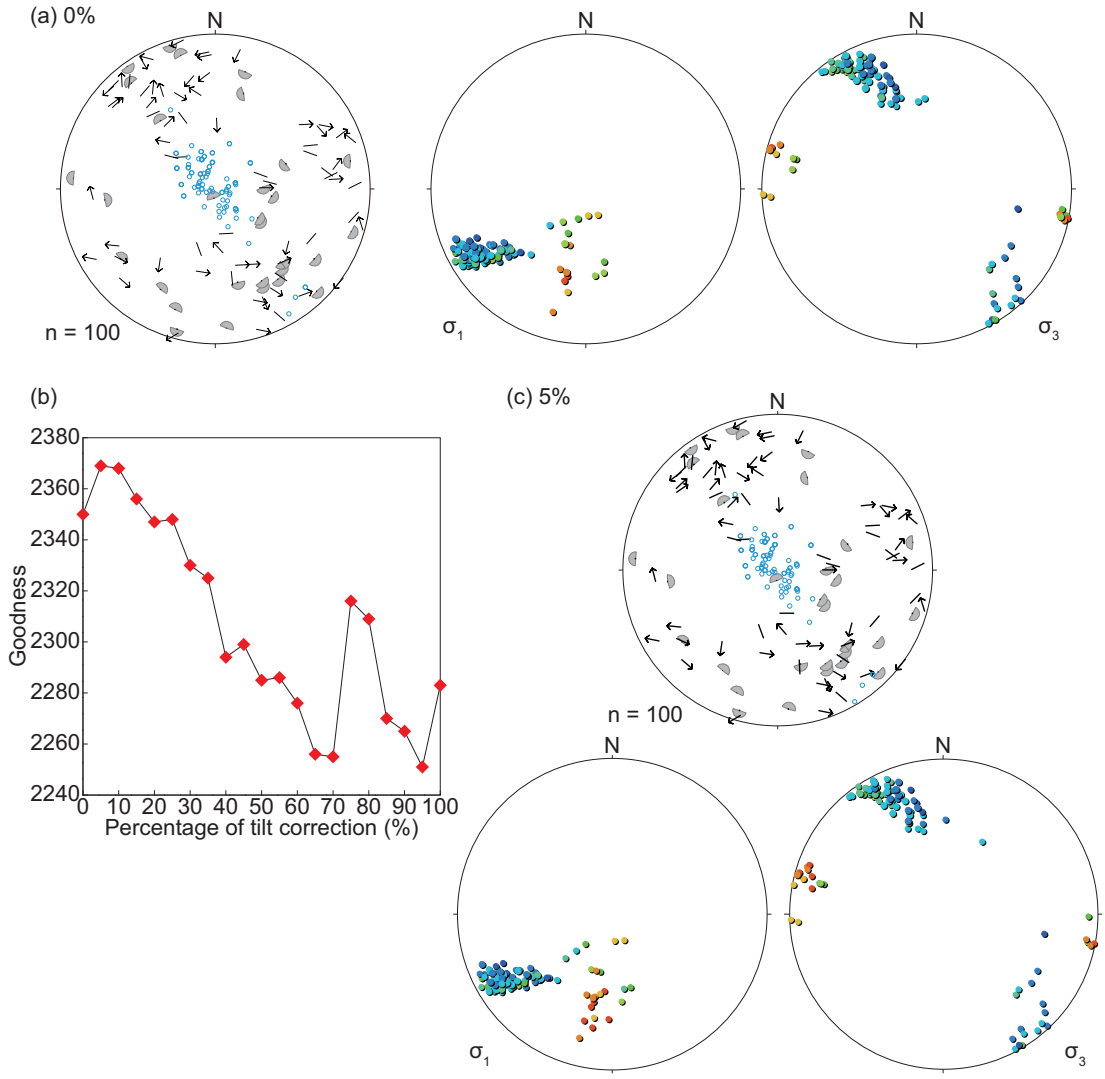

Fig. 21: Outcrop-scale fault data unexplained by Stress Kf-α in the Kurami Group and analysis results. (a) data and the analysis result for original attitudes. (b) a plot of goodness for each stage of tilt correction. (c) data and the analysis result after 5% tilt correction. Legends are the same as Fig. 20.

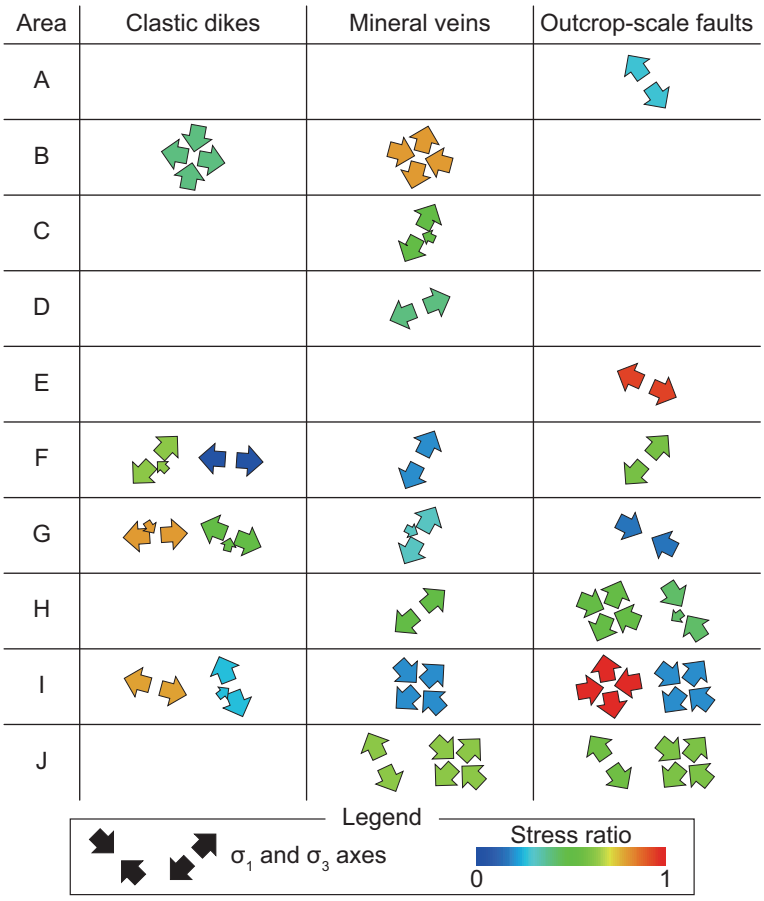

Fig. 22: List of detected stresses in the Tanabe Group. Each arrow shows a non-vertical maximum and minimum principal stress axis. Small arrows mean plunging of the axes. Each row corresponds to the area, and each column corresponds to the structure.

5 Stress Histories

5.1 The Tanabe Group

After the analyses, 26 stresses were detected in the Tanabe Group (Fig. 22). Detected stresses were classified for constructing stress history in the Tanabe Group.

5.1.1 Group X: stresses with E–W trending σ_3 detected from clastic dikes

In all areas where clastic dikes were observed (areas B, F, G, and I), stresses with E–W trending σ_3 axis were detected. They took various stress regimes, such as normal faulting

(stresses Fd-β and Id-α), strike-slip faulting (Stress Bd-α), and σ_1-plunging (stresses Gd-α and Gd-β).

Clastic dikes would have intruded during or soon after the deposition of the Shirahama Formation for the following reasons. First, in the Shirahama Formation, mud-volcanic deposits intercalate (Nakaya and Hamada, 2009), suggesting syn-depositional activities of mud volcanoes. Second, clastic dikes tend to intrude perpendicularly to the bedding (Miyata et al., 2009). Although the bedding tends to tilt gently in many study areas, clastic dikes also intrude perpendicularly to the bedding in Area F (Fig. 14b).

5.1.2 Hierarchical clustering of stresses

Stresses detected from mineral veins and outcrop-scale faults resemble each other in each area, especially in their σ_{Hmax} direction. Such similarity indicates that the timing and depth of formation of veins and faults seem not to be systematically different, although they were not estimated directly.

In order to classify the detected stresses, hierarchical clustering was applied to these stresses. As the dissimilarity of stresses, angular stress distances (Yamaji and Sato, 2006) were used. The distances between clusters were determined by the group average method. After clustering hierarchically, 59.26°, one of the classification criteria of angular stress distance (Yamaji and Sato, 2019), was applied as the threshold for cutting off suborder clusters.

As a result, four clusters were recognized (Fig. 23). Cluster I comprises reverse or strike-slip faulting stresses with NW–SE trending σ_1 axis and small stress ratio ϕ. Cluster II consists of strike-slip faulting stresses with NE–SW trending σ_3 axis and moderate ϕ. Cluster III consists of normal faulting stresses with NE-SW trending σ_3 axis and small to moderate ϕ. Cluster IV consists of normal or strike-slip faulting stress with NNW–SSE trending σ_3 axis and moderate-to-large ϕ.

When focusing on the σ_{Hmax} direction, two groups of clusters can be recognized. One is stresses with NW–SE trending σ_{Hmax} (Group Y), including the clusters I, II, and III. Although their stress regimes vary, the spatial trend can be found. In the southern areas, the stress regime tends to be strike-slip or small ϕ reverse faulting. In the central or northern areas, it tends to be normal or large ϕ strike-slip faulting. The other group is the normal faulting stresses with ENE–SWS trending σ_{Hmax} (NNW–SSE tension stresses, Group Z),

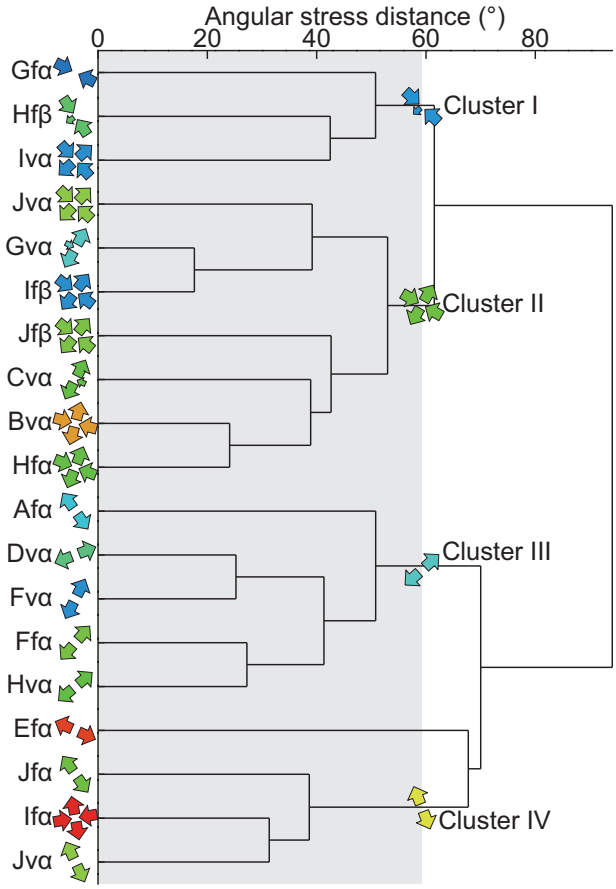

Fig. 23: Dendrogram (the result of hierarchical clustering) of the stresses detected in the Tanabe Group. The legends of stress arrows are the same as Fig. 22.

including Cluster IV. They were detected only in the southern areas (areas I and J).

5.1.3 Stress phases in the Tanabe Group

This study recognized three stress groups: stresses with E–W trending σ_3 (Group X), stresses with NW–SE trending σ_{Hmax} (Group Y), and NNW–SSE tension stresses (Group Z). As mentioned in Section 5.1.1, Group X is considered to have acted in the early middle Miocene of syn-deposition or soon after the deposition of the Shirahama Formation. Stresses belonging to this group were detected in all areas where clastic dikes were observed. This suggests that the group was exerted in the southern and central Tanabe Group and maybe in the whole Tanabe Group. Yielding foraminifers indicated that the Asso Formation was deposited in Wade et al.'s (2011) M5b zone (Section 2.2). U–Pb ages of detrital

zircon suggested that the Shirahama Formation had been deposited before 15 Ma (Section 3). Therefore, Group X should have acted approximately between 16 Ma and 15 Ma and may also have acted before 16 Ma (Fig. 24).

Stresses of Group Y were detected in many of the study areas, with no spatial deviation. Therefore, Group Y is considered to have acted in the whole Tanabe Group. In Area F, Stress Fd-α, belonging to Group Y, was detected. Because of the perpendicularity of dikes to bedding in Area F, Group Y should have acted before tilting. Quartz veins were also measured in the Kumano Group (Miura, 2005; Yamanaka, 2016) and in the basement accretionary complex (Nakaya et al., 2012). In the central and northern Kumano Group, quartz veins were injected in the NW–SE direction, indicating the NW–SE trending σ_{Hmax} axis (Fig. 25). This study reveals that NW–SE striking veins are distributed not only in the central and northern Kumano Group but also in the Tanabe Group.

The cross-cutting relationships of outcrop-scale structures (Section 4.3.4) suggest the order of groups X and Y. Stress Fd-β acted before Stress Fd-α. Stress Gd-α or Gd-β was before Stress Gv-α. Stress Id-α was before Stress Iv-α. All these relationships indicate Group Y acted after Group X. Ishihara Sangyo Kaisha, Ltd. (1984) reported the K–Ar age of adularia of 14.5 ± 0.7 Ma from quartz veins in the Kishu Mine in the central Kumano Group. Stresses detected from mineral veins mainly belong to Group Y, and its timing would correspond to vein injections in the central Kumano Group. Therefore, the stress state in the Tanabe Group should have changed from Group X to Group Y at approximately 15 Ma between the deposition of the Tanabe Group and vein injection (Fig. 24).

Group X was detected only from clastic dikes, whereas Group Y was detected mainly from mineral veins and outcrop-scale faults. Such segregation of clastic dikes and mineral veins suggests their asynchronous formations. The difference in fluid source may caused it. A fault is formed under significant differential stress conditions. The affiliation tendency of stresses detected from outcrop-scale faults suggests that, as stress changes, differential stress would have increased. These segregations also indicate the effectiveness of structural variety for paleo-stress estimation, as mentioned in Section 1.3.

Stresses of Group Z have been detected in the southern Tanabe Group. Therefore, Group Z probably acted only in the southern areas. Group Z has no constraints for its age. However, Stress Id-α belonging to Group X acted before Stress Id-β belonging to Group Z (Section 4.3.4), suggesting that Group Z acted after Group X (Fig. 24). Note that groups Y

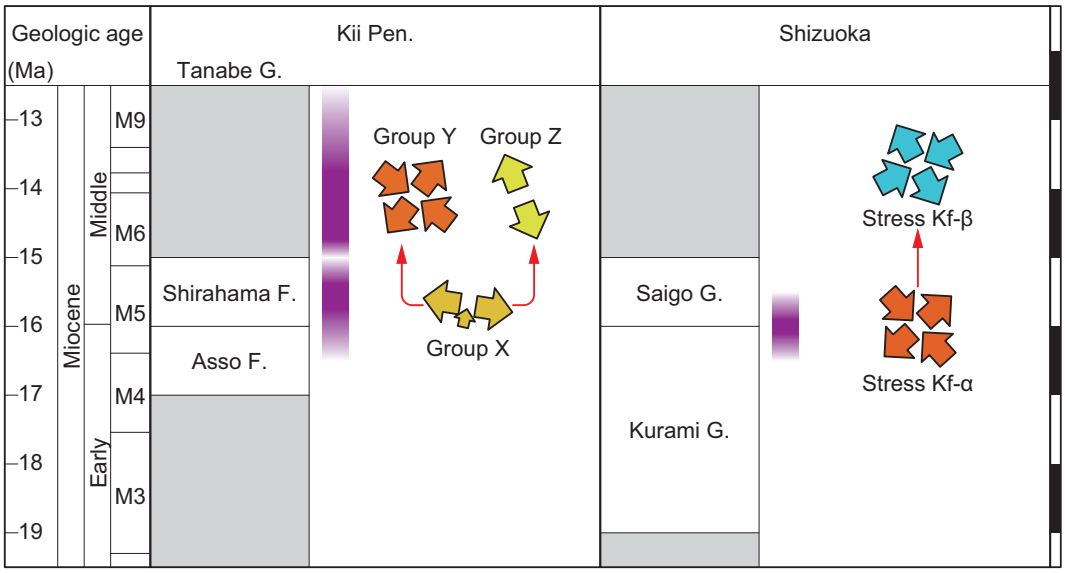

Fig. 24: Stress histories in the Tanabe and Kurami groups. The legends of stress arrows are the same as Fig. 22. Abbreviations: G. (Group) and F. (Formation).

and Z are unknown for their order, and they may have also acted alternately.

5.2 The Kurami Group

In the Kurami Group, two stresses were detected: NE–SW axial tension stress (Stress Kf-α) and ENE–WSW compression strike-slip faulting stress (Stress Kf-β). NE–SW foldings characterize the Kurami Group. Stress Kf-α acted during the folding of the Kurami Group, and Stress Kf-β acted at the end of or after the folding. The Saigo Group is not folded (Fig. 6c), indicating that the folding occurred between the deposition of the Kurami and the Saigo groups. Previous studies reported foraminifers correlated to Blow's (1969) N8 zone from both groups (Saito, 1960; Ibaraki, 1986; Shiba et al., 2020). Therefore, the Kurami Group should be folded, contemporary with Stress Kf-α, at about 16 Ma (Fig. 24). Note that the age of changing stress is not constrained.

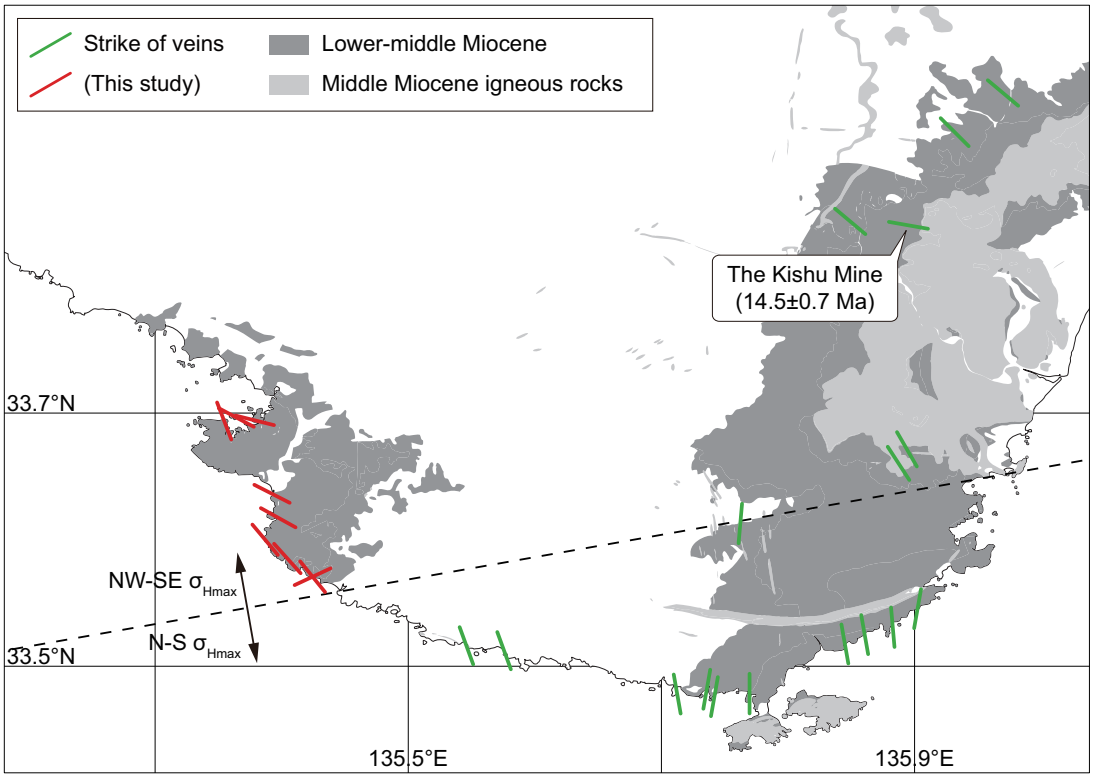

Fig. 25: Strikes of mineral veins in the southern Kii Peninsula. Red bars correspond to data measured in this study, and blue bars correspond to data from previous studies (Nakaya et al., 2012; Yamanaka, 2016). The age of the Kishu Mine quartz veins is after Ishihara Sangyo Kaisha, Ltd. (1984). σ_{Hmax} axes in the southernmost Kii Peninsula direct N–S. On the other hand, those in the Tanabe Group and the central and northern Kumano Group direct NW–SE.

6 Discussion

6.1 Comparison of stress direction in southwest Japan

As mentioned in Section 1.2, it is controversial when stress has changed in middle Miocene southwest Japan. The Japan Sea opening, as one of the most important tectonic changes, is recently considered to have terminated at 15.8 Ma (Hoshi et al., 2015), different from conventional kinematic models (e.g., Otofuji et al., 1985). On the other hand, massive igneous activities are still considered to have started at approximately 15 Ma, according to recent radiometric dating (Shinjoe et al., 2019; Sato and Haji, 2021). Tectonics influences activities in the caldera volcanoes (Houghton et al., 1995), and the start of the activities may reflect the change in stress.

Paying attention to trends of dike swarms (Fig. 26), we can divide southwest Japan into three stress domains: backarc, inner Setouchi, and near-trench. The backarc domain underwent stresses mainly related to the Japan Sea opening. Before 16 Ma, approximately E-W trending dike swarms intruded mainly in the Hokuriku district. Besides the Hokuriku district, dike swarms intruded even in the Tajima area (5 of Table 1; Wadatsumi and Matsumoto, 1958). Haji and Yamaji (2021) analyzed the dikes and outcrop-scale faults, and NE-SW tension stresses were detected. Dike trends, however, vary in all directions, and the intrusion ages also vary between 17.1–13.7 Ma. These facts may be explained by following two explanations. (1) Dikes have intruded under heterogeneous stresses, including those before and after the change. (2) Dike trends show radial distribution representing local stress around a volcanic vent. In addition, some outcrop-scale faults have a reverse sense and seem not to be explained by the optimum normal faulting stress alone. Even if detected stresses acted, they have small stress ratios and may resemble E-W tension stresses reported in the Hokuriku district. Therefore, the stress detected in the Tajima area can be regarded as an exception, and stress with E-W trending σ_{Hmax} would have been dominant in the backarc domain. Dike swarms between 16–15 Ma are limited to the Tajima area. After 15 Ma, N-S trending dike swarms intruded mainly in the San'in district. Thus, the stress in the backarc domain would have changed between 16–15 Ma, although its timing cannot be identified strictly. In the inner Setouchi domain, dikes intruded only after ca. 15 Ma in the E-W (or MTL-parallel) direction, except for a data of 16.5 Ma in the Shitara area (Tsunakawa et al., 1983). In the near-trench domain, dikes intruded in the N-S (or trench-perpendicular)

direction only after ca. 15 Ma.

This study revealed, in the Kurami Group, NE-SW axial tension (Stress Kf-α) had acted at ca. 16 Ma (Fig. 26a). Based on the discussion of Hoshi (2018), the Kurami Group has uncertainty about whether the detected stress holds its original direction or not because of inconsistent paleomagnetic measurement results (Hayashida, 1994; Hiroki and Matsumoto, 1999). Paleomagnetic data reported by Hayashida (1994) suggest counterclockwise rotation of the Kurami Group with reference to Mizunami (Hoshi et al., 2015) and Kani (Hayashida et al., 1991) areas located northwest of the Kurami Group. On the other hand, the data of Hiroki and Matsumoto (1999) indicate no rotation of the Kurami Group with reference to the Mizunami and the Kani areas. Regardless of whether or not the Kurami Group rotated counterclockwise after the deposition, the stress direction in the Kurami Group is different from those in the Hokuriku district of the backarc domain and the Shitara area of the inner Setouchi domain.

In the Tanabe Group, stress with E-W trending σ_3 (Group X) axis acted during or soon after the deposition of the Shirahama Formation, probably before 15 Ma (Fig. 26a, c). In the near-trench domain, stresses with N-S trending σ_{Hmax} axis have been reported only after 15 Ma (Murakami et al., 1989; Haji et al., 2022). Group X suggests that such stress acted not only after 15 Ma but before 15 Ma in the near-trench domain, earlier than the changing of stress ever assumed. Against the conventional description of uniform stress through the southwest Japan arc, both Stress Kf-α and Group X suggest that stresses differ between the forearc domain and the other domains before and after 15 Ma.

After 15 Ma, stress with NW-SE trending σ_{Hmax} (Group Y) acted after the deposition of the Shirahama Formation (Fig. 26b, d). As mentioned in Section 5.1.3, this stress also acted in the central and northern Kumano Group (Fig. 25). On the other hand, previous studies reported N-S trending quartz veins (Miura, 2005; Nakaya et al., 2012; Yamanaka, 2016) and igneous dikes (Haji et al., 2022) in the southern Kumano Group and the basement accretionary prism in the southernmost Kii Peninsula. Radiometric ages were reported from N-S trending igneous dikes (Hoshi et al., 2003; Haji et al., 2022). These ages are similar to the age of NW-SE trending veins (Ishihara Sangyo Kaisha, Ltd., 1984), suggesting the simultaneity of the formation of NW-SE trending veins and N-S trending igneous dikes. Therefore, σ_{Hmax} direction in the Tanabe and central and northern Kumano groups differ from those in the southernmost Kii Peninsula (near-trench domain). After 15 Ma, σ_{Hmax} di-

rection in the inner Setouchi domain was perpendicular to those in the near-trench domain. NW-SE trending σ_{Hmax} would be an intermediate direction between the inner Setouchi and the near-trench domains. In other words, the Tanabe and the central and northern Kumano groups might be the transitional zone of stress between the inner Setouchi and the near-trench domains.

6.2 Tectonic implications

Paying attention to the near-trench stress domain with trench-perpendicular σ_{Hmax} in the Kii Peninsula, their northern limit seems to have retreated trenchward at 15 Ma (Fig. 26c, d). It means the occurrence of stress discontinuity at the south of the Tanabe and the central Kumano groups at 15 Ma, at least on the scale of the Kii Peninsula. The following structures can explain such a spatiotemporal stress change: continental arc basement (Byrne et al., 1993) as a static backstop, out-of-sequence thrust as a dynamic backstop (Kopp and Kukowski, 2003), and intermittent activity of slow earthquake (McNamara et al., 2021). Especially the activity of the out-of-sequence thrust has been implied in other regions. Kishu Shimanto Research Group (2011) suggested the existence of out-of-sequence thrust in the southern Kumano Group because of the intrusion of mud diapirs and their position near the axis of the overturned anticline in the southern Kumano Group. Kozagawa Dike cut folds in the Kumano Group, and thus overturned anticline was formed before the intrusion of the Kozagawa Dike (Hisatomi, 1981) at 14.6±0.2 Ma (Iwano et al., 2007). Additionally, the southern Kumano Group is well folded with a short wavelength, whereas the central and northern Kumano Group shows gentle dipping and is weakly folded (Hisatomi, 1981). Out-of-sequence thrust can explain the strain's spatial difference by performing as strain discontinuity.

In central Japan, the Kanto Syntaxis began to grow before 15 Ma by the collision of the Honshu and the Izu-Bonin-Mariana arcs (Hoshi, 2018). On the western side of the Kanto Syntaxis, N-S trending sinistral strike-slip faults with the reverse component run, such as Akaichi Tectonic Line, Komyo Fault (Kimura, 1959), Sasayama Tectonic Line (Mochizuki et al., 1956; Matsuda and Sugiyama, 2014), and Ikawa-Okaramatsuyama Fault (Yamada et al., 1983; Kano et al., 1986). The region sandwiched by Akaishi Tectonic Line and Komyo Fault is called the Akaishi Tectonic Zone and is considered a strike-slip duplex (Woodcock and Fisher, 1986), having acted from the early to middle Miocene (Kano, 1993). Sasayama

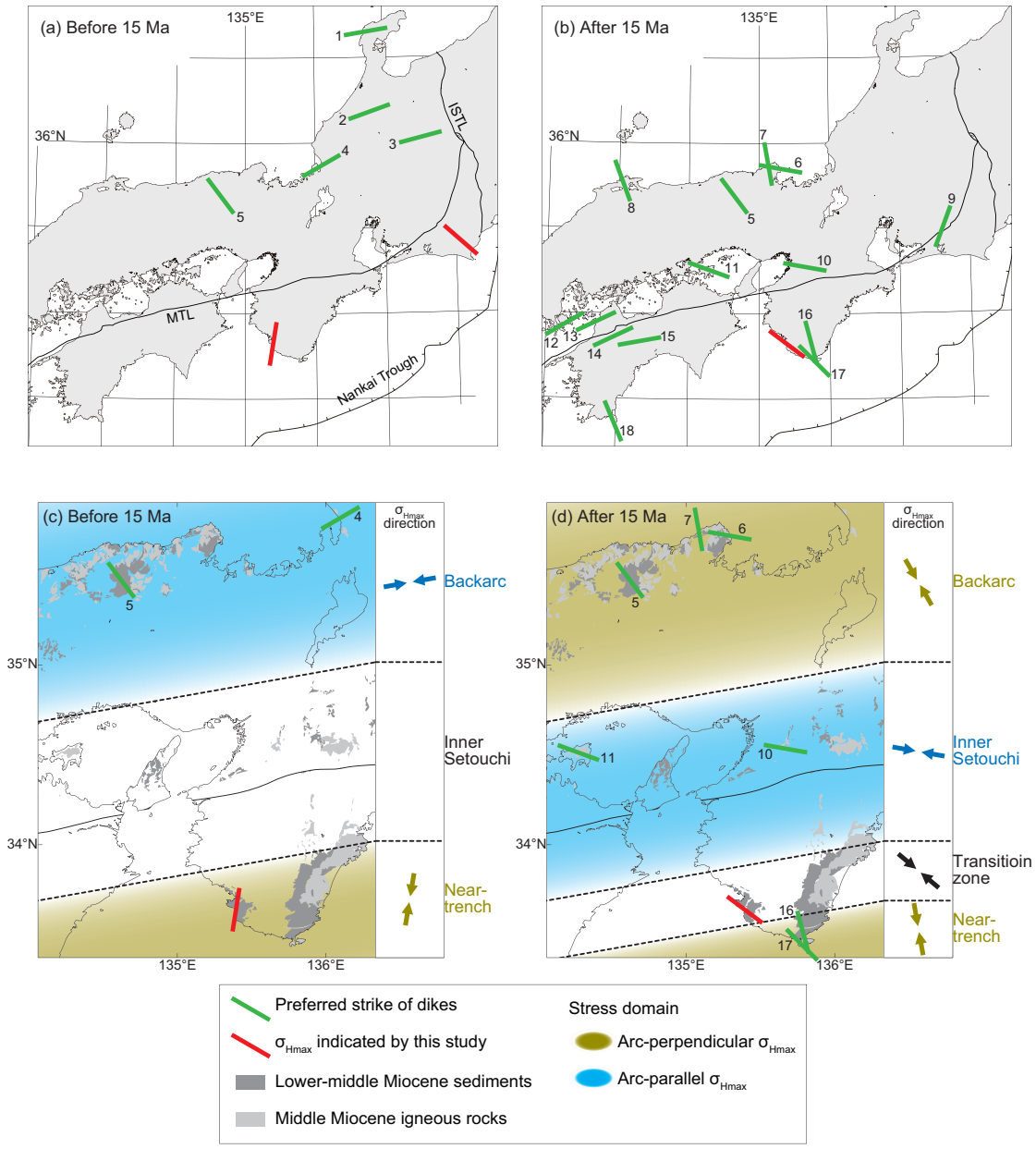

Fig. 26: Stress orientations in southwest Japan (a) before and (b) after 15 Ma, and those with stress domains around the Kinki district (c) before and (d) after 15 Ma, including the data of this study. The indexes of dike swarms correspond to Table 1.

Tectonic Line and Ikawa-Okaramatsuyama Fault are cut by Kaikomagatake granitoid pluton (approximately 15 Ma; Sato et al., 1989), suggesting the faults have been activated mainly before 15 Ma. Sasayama Tectonic Line cuts the Setogawa Group before and after 20 Ma (e.g., Kitazato, 1980), suggesting the fault has been activated mainly after 20 Ma. This study detected NE-SW axial tension stress (Stress Kf-α) from the Kurami Group and estimated that the stress acted during the formation of folds with NE-SW trending axes in the Kurami Group. This study estimated the age of folding and acting of Stress Kf-α as around 16 Ma, consistent with the formation timing of N–S trending sinistral strike-slip faults. The folds may array in the echelon and be formed under Stress Kf-α of sinistral transpressional tectonics.

7 Summary

To reveal how the spatiotemporal variation of forearc stress is recorded, this study conducted paleo-stress analyses for outcrop-scale deformation structures in the lower-middle Miocene forearc basins.

In the Tanabe Group, clastic dikes, mineral veins, and outcrop-scale faults were measured and analyzed for each several kilometers-scale subarea. After the hierarchical clustering of detected stresses, three groups were recognized: stresses with E-W trending σ_3 (Group X), stresses with NW-SE trending σ_{Hmax} (Group Y), and NNW-SSE tension stresses (Group Z). Based on cross-cutting relationships of the structures, comparison with stresses in other regions, and dating of structures in other regions, it was indicated that stress in the Tanabe Group changed from Group X to Group Y at ca. 15 Ma, and Group Z also acted only in the southern Tanabe Group.

In the Kurami Group, outcrop-scale faults were measured and analyzed, and two stresses were detected: NE-SW axial tension stress (Stress Kf-α) and ENE-WSW compression strike-slip faulting stress (Kf-β). A tilting correction test for the faults revealed that Stress Kf-α had acted during folding at ca. 16 Ma, and Stress Kf-β had been exerted after folding.

Against the conventional description of stresses in southwest Japan, this study revealed that stresses before 15 Ma were different between the near-trench and the other stress domains. Stress change in the Tanabe Group indicates the trenchward retreat of the northern boundary of the near-trench stress domain. Such a change may reflect the occurrence of out-of-sequence thrust as a dynamic backstop.

Acknowledgments

I sincerely thank Katsushi Sato for his long-term and compassionate guidance. Atsushi Yamaji gave me a lot of appropriate and crucial advice. I gratefully acknowledge the work of past and present members of the Biosphere Group and also of the Department of Geology and Mineralogy. Toshiki Haji, Harisma, Takafumi Hirata, Toru Nakajima, Sota Niki, Kota Suzuki, and Masaki Takaya have taught the procedures and have given me advice about detrital zircon U-Pb dating. Hiroe Ito and the Department of Geology and Mineralogy office have assisted with my usual research. Tetsuo Kawakami and Akito Tsutsumi gave me helpful comments on the manuscript. I am gratuful to all of the above people.

To collect samples in the designated area of the national natural monument 'Paleo-ripple marks in the Shirahama', I got permission from the Wakayama Prefectural Board of Education (Wakayama Prefectural Directive 04040003-24). This study was financially supported by the Fukada Geological Institute.

References

Abe, N., Sato, K., 2021. Regional and local paleostresses detected from orientations of clastic dikes around mud diapirs in the Miocene Tanabe Group, southwest Japan. *J. Geol. Soc. Japan*, **127**, 709–725.

Asada, M., Moore, G. F., Kawamura, K., Noguchi, T., 2021. Mud volcano possibly linked to seismogenic faults in the Kumano Basin, Nankai Trough, Japan. *Mar. Geophys. Res.*, **42**, doi: 10.1007/s11001-020-09425-7.

Baer, G., Beyth, M., Reches, Z., 1994. Dikes emplaced into fractured basement, Timna Igneous Complex, Israel. *J. Geophys. Res.*, **99**, 24039–24050.

Balázs, A., Faccenna, C., Gerya, T., Ueda, K., Funiciello, F., 2022. The dynamics of forearc – back-arc basin subsidence: Numerical models and observations from Mediterranean subduction zones. *Tectonics*, **41**, doi: 10.1029/2021TC007078.

Bingham, C., 1974. An antipodally symmetric distribution on the sphere. *Ann. Stat.*, **2**, 1201–1225.

Blow, W. H., 1969. Late middle Eocene to recent planktonic foraminiferal biostratigraphy. *In* Brönniman, P., Renz, H. H. eds., *Proceedings of the First International Conference on Planktonic Microfossils, Geneva, 1967*, **1**, 199–422.

Bott, M. H. P., 1959. The mechanics of oblique slip faulting. *Geol. Mag.*, **96**, 109–117.

Byrne, D. E., Wang, W.-H., Davis, D. M., 1993. Mechanical role of backstops in the growth of forearcs. *Tectonics*, **12**, 123–144.

Chemenda, A., Lallemand, S., Bokun, A., 2000. Strain partitioning and interplate friction in oblique subduction zones: Constraints provided by experimental modeling. *J. Geophys. Res.*, **105**, 5567–5581.

Cho, H., Son, M., Sohn, Y. K., Park, M. E., 2017. Magnetic fabric (anisotropy of magnetic susceptibility) constraints on emplacement mechanism of clastic dikes. *J. Geophys. Res.*, **122**, 3306–3333.

Choi, P.-Y., Nakae, S., Kim, H., 2011. Fault tectonic analysis of Kii peninsula, Southwest Japan: Preliminary approach to Neogene paleostress sequence near the Nankai subduction zone. *Isl. Arc*, **20**, 455–476.

Dahlen, F. A., 1990. Critical taper model of fold-and-thrust belts and accretionary wedges. *Annu. Rev. Earth Planet. Sci.*, **18**, 55–99.

Davies, R. J., Huuse, M., Hirst, P., Cartwright, J., Yang, Y., 2006. Giant clastic intrusions primed by silica diagenesis. *Geology*, **34**, 917–920.

Delaney, P. T., Pollard, D. D., Zioney, J. I., McKee, E. H., 1986. Field relations between dykes and joints: Emplacement processes and paleostress analysis. *J. Geophys. Res.*, **91**, 4920–4938.

Dominguez, S., Malavieille, J., Lallemand, S. E., 2000. Deformation of accretionary wedges in response to seamount subduction: Insights from sandbox experiments. *Tectonics*, **19**, 182–196.

Haji, T., Yamaji, A., 2020. Termination of intra-arc rifting at ca 16 Ma in the Southwest Japan arc: The tectonostratigraphy of the Hokutan Group. *Isl. Arc*, **29**, doi: 10.1111/iar.12366.

Haji, T., Yamaji, A., 2021. Post-rift stress history of Southwest Japan inferred from early to middle Miocene intrusions and meso-scale faults in the Tajima-Myokensan area. *Isl. Arc*, **30**, doi: 10.1111/iar.12412.

Haji, T., Yamaji, A., Iwano, H., Danhara, T., Hirata, T., 2022. Extensional stress accompanied by Miocene near-trench magmatism in the southern Kii Peninsula, SW Japan. *J. Asian Earth Sci.*, **235**, doi: 10.1016/j.jseaes.2022.105266.

Haji, T., Yamaji, A., Niki, S., Hirata, T., 2019. Zircon U–Pb age of a lapilli tuff bed in the lower Miocene Yoka Formation, northern Hyogo, SW Japan. *J. Geol. Soc. Japan*, **125**, 867–875.

Harada, T., Nakaya, S., 1999. Hot springs. *Urban Kubota*, **38**, 42–56.

Hayashida, A., 1994. Paleomagnetism of Miocene sedimentary rocks in the Kakegawa area and implication for tectonic rotation in central japan. *J. Geomag. Geoelectr.*, **46**, 1051–1066.

Hayashida, A., Fukui, T., Torii, M., 1991. Paleomagnetism of the early Miocene Kani Group in southwest Japan and its implication for the opening of the Japan Sea. *Geophys. Res. Lett.*, **18**, 1095–1098.

Hildebrandt, C., Egenhoff, S., 2007. Shallow-marine massive sandstone sheets as indicators of palaeoseismic liquefaction: An example from the Ordovician shelf of Central Bolivia. *Sediment. Geol.*, **202**, 581–595.

Hiroki, Y., Matsumoto, R., 1999. Magnetostratigraphic correlation of Miocene regression-and-transgression boundaries in central Honshu, Japan. *J. Geol. Soc. Japan*, **105**, 87–107.

Hisatomi, K., 1981. Geology and sedimentolgy of the Kumano Group in the southeastern part of the Kumano basin, Kii Peninsula. *J. Geo. Soc. Japan*, **87**, 157–174.

Hoshi, H., 2018. Kanto Syntaxis: when did it begin to grow? *J. Geol. Soc. Japan*, **124**, 805–817.

Hoshi, H., Iwano, H., Danhara, T., 2002. Fission-track dating of the Setouchi valcanic rocks: An example from the Nijo Group, Kinki district, southwest Japan. *J. Geol. Soc. Japan*, **108**, 353–365.

Hoshi, H., Iwano, H., Danhara, T., Yoshida, T., 2003. Fission-track dating of the Shionomisaki Igneous Complex, Kii Peninsula, Japan. *J. Geol. Soc. Japan*, **109**, 139–150.

Hoshi, H., Kato, D., Ando, Y., Nakashima, K., 2015. Timing of clockwise rotation of Southwest Japan: constraints from new middle Miocene paleomagnetic results. *Earth Planets Space*, **67**, doi: 10.1186/s40623-015-0266-3.

Hoshi, H., Takagawa, M., 2009. Early Miocene parallel dike swarms in the Tsuruga Bay area, back-arc side of central Japan. *J. Geol. Soc. Japan*, **115**, 96–99.

Houghton, B. F., Wilson, C. J. N., McWilliams, M. O., Lanphere, M. A., Weaver, S. D., Briggs, R. M., Pringle, M. S., 1995. Chronology and dynamics of a large silicic magmatic system: Central Taupo Volcanic Zone, New Zealand. *Geology*, **23**, 13–16.

Resolution of the age structure of the detrital zircon populations of two Lower Creaceous sandstones from the Weald of England by fission track dating. *Geol. Mag.*, **121**, 269–277.

Ibaraki, M., 1986. Planktonic foraminiferal datum levels recognized in the Neogene sequence of the Kakegawa area, and their relationship with the lithostratigraphy. *J. Geol. Soc. Japan*, **92**, 119–134.

Iizuka, T. and Hirata, T., 2004. Simultaneous determinations of U–Pb age and REE abundances for zircons using ArF excimer laser ablation-ICPMS. *Geochem. J.*, **38**, 229–241.

Ikebe, N., Chiji, M., Morozumi, Y., 1975. *Lepidocyclina* horizon in the Miocene Kumano Group in reference to planktonic foraminiferal biostratigraphy. *Bull. Osaka Mus. Nat. Hist.*, **29**, 81–89.

Ishihara Sangyo Kaisha, Ltd., 1984. Progress in exploration at the Kishu Mine. *Mine Exploration in Japan (Nihon no Kosho Tansa)*, **2**, 113–144.*

Ishiwatari, A., Ohama, H., 1997. Clinopyroxene basalt dikes in the Miocene Iwaine Formation, Hokuriku Province, Japan: Various continental arc magmas including shoshonite series and origin of the clinopyroxene phenocrysts. *J. Geol. Soc. Japan*, **103**, 565–578.

Iwano, H., Danhara, T., Hoshi, H., Kawakami, Y., Sumii, T., Shinjoe, H., Wada, Y., 2007. Simultaneity and similarity of the Muro Pyroclastic Flow Deposit and the Kumano Acidic Rocks in Kii Peninsula, southwest Japan, based on fission track ages and morphological characteristcs of zircon. *J. Geol. Soc. Japan*, **113**, 326–339.

Iwano, H., Orihashi, Y., Hirata, T., Ogasawara, M., Danhara, T., Horie, K.,⋯Yamamoto, K., 2013. An inter-laboratory evaluation of OD-3 zircon for use as a secondary U–Pb dating standard. *Isl. Arc*, **22**, 382–394.

Jackson, S. E., Pearson, N. J., Griffin, W. L., Belousova, E. A., 2004. The application of laser ablation-inductively coupled plasma-mass spectrometry to in situ U–Pb zircon geochronology. *Chem. Geol.*, **211**, 47–69.

Jochum, K. P., Pfänder, J., Woodhead, J. D., Willbold, M., Stoll, B., Herwig, K.,... Hofmann, A. W., 2005. MPI-DING glasses: New geological reference materials for in situ Pb isotope analysis. *Geochem. Geophys. Geosyst.*, **6**, Q10008, doi: 10.1029/2005GC000995.

Kano, K., Tanaka, H., Yoshida, T., Matsui, N., 1993. Formation of the Akaishi Tectonic Zone and its significance on the crustal reconstruction of the eastern part of Southwest Japan Arc during the Miocene. *Mem. Geol. Soc. Japan*, **42**, 203–223.

Kano, K., Muramatsu, T., Hirota, Y., 1986. Deformation style of the upper Cretaceous Shimanto Supergroup in the southern Akaishi mountains, central Japan. *Geosci. Rep. Shizuoka Univ.*, **12**, 89–114.

Kano, K., Yoshida, F., 1985. *Geology of the Sakaiminato district*. Quadrangle Series, scale 1:50,000, Geol. Surv. Japan, 57p.

Kimura, K., 1985. Stratigraphy and sedimentary facies of the Tertiary Shimizu and Misaki Formations in the southwestern part of Shikoku. *J. Geol. Soc. Japan*, **91**, 815–831.

Kimura, T., 1959. Shrap bent of the Median Tectonic Line and its relation to the Akaishi Tectonic Line: tectonic significances yielded by lateral faults. *J. Geol. Geogr.*, **30**, 215–232.

Kimura, J., Stern, R. J., Yoshida, T., 205. Reinitiation of subduction and magmatic responses in SW Japan during Neogene time. *Geol. Soc. Am. Bull.*, **117**, 969–986.

Kinoshita, H., Yamaji, A., 2021. Arc-parallel extension in preparation of the rotation of southwest Japan: Tectonostratigraphy and structures of the Lower Miocene Ichishi Group. *Isl. Arc*, **30**, doi: 10.1111/iar.12418.

Kishu Shimanto Research Group, 2011. Mud diapirs of the Miocene Kumano Group in the Kii Peninsula, Southwest Japan, with spacial reference to their relation to the Mega Splay Faults on the southern margin of the Miocene forearc basin: The study of the

Shimanto terrain in the Kii Peninsula, southwest Japan (Part 15). *Earth Sci. (Chikyu Kagaku)*, **65**, 1–16.

Kitazato, H., 1980. Deep sea benthonic foraminiferal assemblage of the Setogawa Group. *In* Taira, A., Tashiro, M., eds., *Geology and oaleontology of the SHimanto Belt: Selected Papers in Honor of Prof. Jiro Katto*, Rinyakosaikai Press, Kochi, 219–225.

Kobayashi, Y., 1979. Early and middle Miocene dike swarms and regional tectonic stress field in the southwest Japan. *Volcanol. Soc. Japan*, **24**, 203–212.

Kobayashi, H., Yamaji, A., Masuda, F., 2005. Miocene stratigraphy, sedimentary environments and tectonics in the Wajima area, Noto Peninsula, southern margin of the Japan Sea. *J. Geol. Soc. Japan*, **111**, 286–299.

Kopp, H., Kukowski, N., 2003. Backstop geometry and accretionary mechanics of the Sunda margin. *Tectonics*, **22**, doi: 10.1029/2002TC001420.

Kusuhashi, N., Yamaji, A., 2001. Miocene tectonics of SW Japan as inferred from the Kuma Group, Shikoku. *J. Geol. Soc. Japan*, **107**, 26–40.

Marshall, J. D., Pirrie, D., 2013. Carbonate concretions–explained. *Geol. Today*, **29**, 53–62.

Martin, K. M., Gulick, S. P. S., Bangs, N. L. B., Moore, G. F., Ashi, J., Park, J.-O.,... Taira, A., 2010. Possible strain partitioning structure between the Kumano fore-arc basin and the slope of the Nankai Trough accretionary prism. *Geochem. Geophys. Geosyst.*, **11**, doi: 10.1029/2009GC002668.

Matsuda, T., Sugiyama, Y., 2014. Geology of the Nanbu District, 10. Geological structures. *Quadrangle Series, 1:50,000*, Geological Survey of Japan, AIST, 96–115.

McNamara, D. D., Behboudi, E., Wallace, L., Saffer, D., Cook, A. E., Fagereng, A.,... Petronotis, K. E., 2021. Variable In Situ Stress Orientations Across the Northern Hikurangi Subduction Margin. *Geophys. Res. Lett.*, **48**, doi: 10.1029/2020gl091707.

Miura, D., 2005. Effects of changing stress states on the development of caldera-bounding faults: Geological evidence from Kumano caldera, Japan. *J. Volcanol. Geotherm. Res.*, **144**, 89–103.

Miyata, Y., Miyake, K., Tanaka, K., 2009. Mud diapirs and associated intrusion structures in the Miocene Tanabe Group. *J. Geol. Soc. Japan*, **115**, 470–482.

Mochizuki, K., Samejima, T., Takeuchi, M., Kato, Y., Tsuchi, R., 1956. Geology of Shizuoka Prefecture and 1:200,000 scale geological map of Shizuoka Prefecture. Shizuoka Prefecture, Shizuoka, 57p.

Mosher, D. C., Austin, J. A., Fisher, D., Gulick, S. P. S., 2008. Deformation of the northern Sumatra accretionary prism from high-resolution seismic reflection profiles and ROV observations. *Mar. Geol.*, **252**, 89–99.

Murakami, N., Imaoka, T., Uozumi, S., 1989. Ring complex of the Cape of Ashizuri, and its mode of emplacement, Kochi Prefecture, Southwest Japan. *Monogr. Assoc. Geol. Collab. Japan*, **36**, 115–142.

Nakajima, T., 2018. Tectonics of sedimentary basins in and around Japan since the opening of the Sea of Japan. *J. Geol. Soc. Japan*, **124**, 693–722.

Nakajima, T., Yoshikawa, K., Okitsu, O., 2021. Geologic structures and basin formation tectonics in and around Toyama Trough, the Sea of Japan. *J. Geol. Soc. Japan*, **127**, 165–188.

Nakaya, S., Hamada, Y., 2009. Paleo-mud-volcanoes of the Lower Miocene Tanabe Group on the southern Kii Peninsula, southwest Japan. *J. Geogr.*, **118**, 472–491.

Nakaya, S., Suzuki, H., Takesue, Y., 2012. Middle Miocene igneous rocks and hot-temperature springs in the southern part of the Kii Peninsula, Southwest Japan. *Monogr., Assoc. Geol. Collab. Japan*, **59**, 249–261.

Nishimura, A., Miyake, Y., 1973. Occurence of *Lepidocyclina* and *Miogypsina* in the Kumano Group. *In: Collection of Papers of Shimanto Geosyncline Symposium*, 37–38.

Noda, A., 2016. Forearc basins: Types, geometries, and relationships to subduction zone dynamics. *Geol. Soc. Am. Bull.*, **128**, 879–895.

Otofuji, Y., Hayashida, A., Torii, M., 1985. When was the Japan Sea opened?: Paleomagnetic evidence from Wouthwest Japan. *In* Nasu, N., Uyeda, S., Kobayashi, K.,

Kushiro, I., Kagami, H., eds., *Formation of Active Ocean Margins*, Terrapub, Tokyo, 551–566.

Otsubo, M., Shigematsu, N., Kitagawa, Y., Koizumi, N., 2009. Stress history in the forearc region of the Nankai trough subduction zone: paleostress analysis based on faults in core samples from the Kumano Ichiura and Kihoku Miyama sites, Kii Peninsula, SW Japan. *J. Geol. Soc. Japan*, **115**, 457–469.

Ozaki, M., 2009. Tectonic evolution during Eocene to Miocene. *In* Geological Society of Japan, eds., *Monogr. Geol. Japan, Vol. 5, Kinki*, Asakura Publ., Tokyo, 43–61.

Park, J. O., Tsuru, T., Kodaira, S., Cummins, P. R., Kaneda, Y., 2002. Splay fault branching along the Nankai subduction zone. *Science*, **297**, 1157–1160.

Raffi, I., Wade, B. S., Pälike, H., 2020. The Neogene Period. *In* Gradstein, F. M., Ogg, J. G., Schmitz, M. D. and Ogg, G. M., eds., *Geologic Time Scale 2020*, Elsevier, Amsterdam, 1141–1215.

Saito, T., 1960. Tertiary Stratigraphy of the Kakegawa District, Central Japan and its Planktonic Foraminifera. *Contrib. Inst. Geol. Paleontol. Tohoku Univ.*, **51**, 1–45.

Sato, K., 2006. Incorporation of incomplete fault-slip data into stress tensor inversion. *Tectonophysics*, **421**, 319–330.

Sato, D., Haji, T., 2021. Tectonic setting and formation of the Setouchi volcanic rocks in the western Seto Inland Sea, Japan. *Isl. Arc*, **30**, doi: 10.1111/iar.12405.

Sato, K., Shibata, K., Uchiumi, S., 1989. K–Ar ages and cooling history of the Kaikomagatake granitoid plutons, and their bearing on tectonic evolution of the Akaishi Mountains, central Japan. *J. Geol. Soc. Japan*, **95**, 33–44.

Sato, K., Yamaji, A., Tonai, S., 2013. Parametric and non-parametric statistical approaches to the determination of paleostress from dilatant fractures: Application to an Early Miocene dike swarm in central Japan. *Tectonophysics*, **588**, 69–81.

Schellart, W. P., Moresi, L., 2013. A new driving mechanism for backarc extension and backarc shorteing through slab sinnking induced toroidal and poloidal mantle flow:

Results from dynamic subduction models with an overriding plate. *J. Geol. Res.*, **118**, 3221–3248.

Shiba, M., Yokoyama, K., Ohashi, T., Morizumi, M., Maekawa, K., Kondo, T., Ogi, N., 2020. Stratigraphy and sedimentary processes of the Miocene Kurami and Saigo Groups, Shizuoka Prefecture, Japan. *Earth Sci. (Chikyu Kagaku)*, **74**, 137–155.

Shimizu, H., 1985. Pebbly mudstone diapirs of the Tanabe Group in the Kii Pninsula, southwest Japan. *J. Geol. Soc. Japan*, **91**, 691–697.

Shinjoe, H., Orihashi, Y., Anma, R., 2019. U–Pb ages of Miocene near-trench granitic rocks of the Southwest Japan arc: implications for magmatism related to hot subduction. *Geol. Mag.*, doi: 10.1017/s0016756819000785.

Shinjoe, H., Orihashi, Y., Sumii, T., 2010. U–Pb zircon ages of syenitic and granitic rocks in the Ashizuri igneous complex, southwestern Shikoku: Constraint for the origin of forearc alkaline magmatism. *Geochem. J.*, **44**, 275–283.

Shinjoe, H., Orihashi, Y., Sumii, T., 2017. U–Pb zircon ages of Miocene igneous rocks in western Shikoku. *124th Annu. Meet. Geol. Soc. Japan, Abstr*, 92.

Sugisaki, Y., Hoshi, H., 2017. Geological implications of a paleomagnetic direction obtained from a Miocene dike swarm in the Hida region, central Japan. *J. Geol. Soc. Japan*, **123**, 953–967.

Takada, A., 1988. Subvolcanic structure of the central dike swarm associated with the ring complexes in the Shtara district, central Japan. *Bull. Volcanol.*, **50**, 106–118.

Takano, O., 2017. Intermittent formation, sedimentation and deformation history of Cenozoic forearc basins along the Northwestern Pacific Margins as an indicator of tectonic scenarios. *In* Itoh, Y., Takano, O., Takashima, R., Nishi, H., Yoshida, T., eds., *Dynamics of Arc Migration and Amalgamation-Architectural Examples from the NW Pacific Margin*, IntechOpen, London, 1–24.

Takeshita, T., 1993. Deformation of the forearc region and along the Median Tectonic Line in southwest Japan during the opening of the Japan Sea: A preliminary report. *Mem. Geol. Soc. Japan*, **42**, 225–244.

Tanabe Research Group, 1984. Stratigraphy and geological structure of the Tanabe Group in the Kii Peninsula, Southwest Japan. *Earth Sci. (Chikyu Kagaku)*, **38**, 249–263.

Tanabe Research Group, 1992. Sedimentary facies and stratigraphy of the Asso Formation: Study on the Asso Formation, Tanabe Group (Part 1). *Earth Sci. (Chikyu Kagaku)*, **46**, 369–383.

Tanase, A., Umeda, K., Mizuochi, Y., Ninomiya, A., 2001. K–Ar age of andesite dike swarm distributed in the east of Takayama City, Gifu Prefecture. *108th Annu. Meet. Geol. Soc. Japan, Abstr*, 225.

Tatsumi, Y., Ishikawa, N., Anno, K., Ishizaka, K., Itaya, T., 2001. Tectonic setting of high-Mg andesite magmatism in the SW Japan arc: K–Ar chronology of the Setouchi volcanic belt. *Geophys. J. Int.*, **144**, 625–631.

Tatsumi, Y., Tani, K., Sato, K., Danhara, T., Hyodo, H., Kawabata, H., Hanyu, T., Dunkley, D. J., 2010. Multi-chronology of volcanic rocks leading to reliable age estimates of volcanic activity: an example from the Setouchi volcanic rocks on Shodo-Shima Island, SW Japan. *J. Geol. Soc. Japan*, **116**, 661–679.

Tonai, S., Sato, K., Ashi, J., 2011. Incremental fold test for paleostress analysis using the Hough transform inverse method. *J. Struct. Geol.*, **33**, 1158–1168.

Tsuji, T., Ashi, J., Strasser, M., Kimura, G., 2015. Identification of the static backstop and its influence on the evolution of the accretionary prism in the Nankai Trough. *Earth Planet. Sci. Lett.*, **431**, 15–25.

Tsunakawa, H., Kobayashi, Y., Takada, A., 1983. K–Ar ages of dikes in Southwest Japan. *Geochem. J.*, **17**, 265–268.

Umehara, N., Itaya, T., Yoshikura, S., 1991. K–Ar dating on felsic igneous rocks along the Kamiyakawa-Ikegawa Tectonic Line. *J. Mineral. Petrol. Econ. Geol.*, **86**, 299–304.

Wadatsumi, K., Matsumoto, T., 1958. The stratigraphy of the Neogene formations in northern Tazima: Study of the Neogene in the north-western part of the Kinki District (Part 1). *J. Geol. Soc. Japan*, **64**, 625–637.

Wade, B. S., Pearson, P. N., Berggren, W. A., Pälike, H., 2011. Review and revision of Cenozoic tropical planktonic foraminiferal biostratigraphy and calibration to the geomagnetic polarity and astronomical time scale. *Earth Sci. Rev.*, **104**, 111–142.

Wallace, R. E., 1951. Geometry of shearing stress and relation to faulting. *J. Geol.*, **59**, 118–130.

Wallace, L. M., Fagereng, Å., Ellis, S., 2012. Upper plate tectonic stress state may influence interseismic coupling on subduction megathrusts. *Geology*, **40**, 895–898.

Wang, K., Hu, Y., 2006. Accretionary prisms in subduction earthquake cycles: The theory of dynamic Coulomb wedge. *J. Geophys. Res.*, **111**, doi: 10.1029/2005JB004094.

Wendt, I., Carl, C., 1985. U/Pb dating of discordant 0.1 Ma old secondary U minerals. *Earth Planet. Sci. Lett.*, **73**, 278–284.

Wetherill, G. W., 1956. Discordant uranium–lead ages, I. *Trans. Am. Geophys. Union*, **37**, 320–326.

Wiedenbeck, M., Alle, P., Corfu, F., Griffin, W. L., Meier, M., Oberli, F.,... Spiegel, W., 1995. Three natural zircon standards for U–Th–Pb, Lu–Hf, trace element and ree analyses. *Geostand. Newsl.*, **19**, 1–23.

Woodcock, N. H., Fischer, M., 1986. Strike-slip duplexes. *J. Struct. Geol.*, **8**, 725–735.

Yamada, T., Watanabe, T., Kawachi, Y., Yuasa, M., Sekine, M., Matsu'ura, K.,... Demachi, M., 1983. Geology of the Shimanto Belt of the northern Akaishi mountains, central Japan. *Earth Sci. (Chikyu Kagaku)*, **37**, 329–348.

Yamaji, A., Sato, K., 2006. Distances for the solutions of stress tensor inversion in relation to misfit angles that accompany the solutions. *Geophys. J. Int.*, **167**, 933–942.

Yamaji, A., Sato, K., 2011. Clustering of fracture orientations using a mixed Bingham distribution and its application to paleostress analysis from dike or vein orientations. *J. Struct. Geol.*, **33**, 1148–1157.

Yamaji, A., Sato, K., 2019. Stress inversion meets plasticity theory: A review of the theories of fault-slip analysis from the perspective of the deviatoric stress-strain space. *J. Struct. Geol.*, **125**, 296–310.

Yamaji, A., Sato, K., Tonai, S., 2010. Stochastic modeling for the stress inversion of vein orientations: Paleostress analysis of Pliocene epithermal veins in southwestern Kyushu, Japan. *J. Struct. Geol.*, **32**, 1137–1146.

Yamamoto, T., 1991. Late Cenozoic dyke swarms and tectonic stress field in Japan. *Bull. Geol. Surv. Japan*, **42**, 131–148.

Yamamoto, T., Hoshizumi, H., 1988. Stratigraphy of the Neogene system in the Tango Peninsula, eastern part of the San-in district, Southwest Japan, and associated Middle Miocene volcanism. *J. Geol. Soc. Japan*, **94**, 769–781.

Yamanaka, K., 2016. The position of the triple junction indicated from paleostresses in the Kii Peninsula. *Research Report of Fukada Research Grant 2015*, 31–35.*

Yamanaka, K., Yamaji, A., 2017. Paleostresses detected from mineral veins in the Miocene Kumano Group, Kii peninsula, SW Japan. *124th Annu. Meet. Geol. Soc. Japan, Abstr*, 499.

Yanagisawa, Y., 1999. Diatom biostratigraphy of the Miocene sequence in the Suzu area, Noto Peninsula, Ishikawa Prefecture, central Japan. *Bull. Geol. Surv. Japan*, **50**, 167–213.

Yoshida, H., Ujihara, A., Minami, M., Asahara, Y., Katsuta, N., Yamamoto, K.,... Metcalfe, R., 2015. Early post-mortem formation of carbonate concretions around tusk-shells over week-month timescales. *Sci. Rep.*, **5**, doi: 10.1038/srep14123.

Yoshimura, T., Muramatsu, T., Shirasawa, T., Nishizaka, M., 1989. Fission track age of the Setogawa and the Kurami Group. *96th Annu. Meet. Geol. Soc. Japan, Abstr*, 195.

Zhang, J., Zhang, B., Zhao, H., 2016. Timing of amalgamation of the Alxa Block and the North China Block: Constraints based on detrital zircon U–Pb ages and sedimentologic and structural evidence. *Tectonophysics*, **668–669**, 65–81.

[URL1] Geological Survey of Japan, updated on 10th May, 2019, https://gbank.gsj.jp/seamless/.

* English translation from the original written in Japanese.